Spectrum of Engineering Sciences
ISSN (e) 3007-3138 (p) 3007-312X Volume 3, Issue 11, 2025

INFLUENCE OF EMBEDDED-BEAM GEOMETRY ON SEISMIC PERFORMANCE OF DOUBLE-SKIN COMPOSITE SHEAR WALL (DSCSW) H-SECTION BEAM CONNECTIONS: A PARAMETRIC FINITE-ELEMENT STUDY

Imran Ali Channa[*1], Ubaidullah Khan[2], Aijaz Ali Dahri[3] Muhammad Zain Asghar[*4]

*[*1,2,3]Department of Civil Engineering, Quaid-e-Awam University of Engineering, Science & Technology Nawabshah, Sindh, Pakistan,[4]Department of Civil Engineering, National University of Computer and Emerging Sciences (FAST) University, Lahore, Punjab*

[*1]engrimranalichanna@gmail.com, [2]ubaidullahkhan@quest.edu.pk, [3]aliaijazdahri@gmail.com, [4]m.zain.asghar.331@gmail.com

DOI: https://doi.org/10.5281/zenodo.17556074

Keywords
DSCSW, embedment length, embedment height, hysteresis, finite element, seismic design

Article History
Received: 16 September 2025
Accepted: 26 October 2025
Published: 07 November 2025

Corresponding Author: *
Imran Ali Channa

Abstract
This study investigates the seismic performance of double-skin composite shear wall (DSCSW) connections with embedded H-section steel beams, focusing on the influence of embedment length and height. Thirteen nonlinear finite-element (FE) models were developed and analyzed in ABAQUS, validated against existing experimental results. Two parametric groups were studied: (i) varying embedment length (SL-series: 300–700 mm), and (ii) varying embedment height (SH-series: 250–500 mm). Results showed that increasing embedment length from 300 mm to 700 mm enhanced peak bearing capacity by 21.6% and cumulative energy dissipation by 27.8%, with SL-2 (500 mm length) and SL-4 (600 mm length) providing the most stable hysteretic loops. Conversely, excessive embedment height (500 mm) increased stiffness but reduced ductility, leading to brittle shear failure. The optimal embedment height was 350 mm (SH-2), yielding a 15.4% higher energy dissipation and delaying stiffness degradation by two loading cycles compared to SH-1. Skeleton curve analysis confirmed that plastic hinge formation shifted outward with increased embedment, improving rotation capacity. Overall, parametric results provide quantifiable design guidance: embedment lengths of 500–600 mm and embedment heights of 300–350 mm balance strength, ductility, and energy dissipation, offering a seismic design recommendation for DSCSW–H-beam connections.

1. Introduction

Earthquake engineering has been mainly concerned with the seismic behavior of structural systems especially as high-rise and long-span structural systems have become very popular and demand both strength and ductility. Although conventional reinforced concrete (RC) shear walls are commonly used, their failure modes are brittle, reinforcement congestion is complex and the dissipation of energy in cyclic loading is small. To overcome all these faults, it is suggested that double-skin composite shear walls (DSCSWs) can be an innovative system that consists of two parallel plates composed of steel and a concrete core. Such a structure has increased ductility, better confinement, and less complexity in reinforcement than conventional RC walls. Moreover, the use of embedded steel beams at the wall to beam interface has also developed as an opportunity detail to enhance connection performance to provide a stable hysteresis behavior

and dependable seismic load transfer (Cao et al., 2008).

Although many studies have been involved on global behavior of composite shear walls based on cyclic and monotonic loads, research has been scarcely done on the local behavior of DSCSW-to-beam connections, particularly, paying attention to the geometric embedment of the connections. Past studies have mainly focused on reinforcement anchorage, concrete confinement, and steel plate buckling, but it has not given much attention to the quantitative contribution of the embedment length and height of steel beam. These parameters however, have critical implications on the mechanisms of load transfers, maintenance of stiffness and development of plastic hinges. Lack of explicit design instructions has limited the extended usage of DSCSWs in seismic areas (Wan-Shin and Hyun-Do, 2006). It is in this respect that the current study utilizes a finite-element (FE) analysis method which is parametric in nature to examine how embedded-beam geometry affects DSCSW connections. There was 13 nonlinear FE models developed in ABAQUS which were divided into two parametric groups: different embedment length (300 to 700 mm, SL-series) and different embedment height (250 to 500 mm, SH-series). The models were tested with the benchmark of experiment in order to assure reliability of results. The simulated seismic conditions were cyclic loading, and load-displacement hysteresis, skeleton curves, and stiffness degradation of the performance measures were evaluated systematically (Xiaodong et al., 2017).

The results indicate that the embedment length and the height have a significant influence on the seismic performance of DSCSW-H-beam connections. An increase in the embedment length increases the load capacity and the dissipated energy but causes uneven stress distribution beyond 600 mm. On the other hand, when the embedment height is increased, it enhances initial stiffness and decreases ductility at an excessive height of 400 mm, which is a range of desirable designs. The dual effect highlights the importance of balanced embedment geometry in order to attain seismic resilience (Li, Wang, and Wu, 2018). The research findings of this paper are two-fold. Most importantly, it offers a quantitative evaluation of embedment parameters on the basis of proven FE modeling, which is a knowledge gap in the literature. Second, it presents realistic proposals on the best embedment dimensions that will yield maximum energy dissipation and not affect the ductility. This study provides fundamental information to structural designers by filling the analytical modeling-engineering practice gap, which will help to make DSCSWs a safe and efficient solution in the seismic-prone regions (Guo et al., 2022).

2. Literature Review

To mention a few, the study conducted by Žuvelek et al. was conducted at the College of Civil Engineering, Hunan University, China in collaboration with the State Key Laboratory of Structural Analysis of the Industrial Equipment, Dalian University of Technology in the years 20222023 under the aim to determine the seismic performance of the steel concrete composite shear walls (SCSWs) with new boundary connections. They used experimental testing and nonlinear finite element analysis to find out the influence of connection details on global seismic response. The wall samples of large scale were of size 2000mm in height and 1200 mm in width, made of 6 mm thick faceplates, headed studs and C40 concrete and differed in details of boundary reinforcement and plate anchorage. The mimicking of the earthquake actions was done through cyclic lateral loading tests at constant axial compression ratios (n = 0.2–0.3). Findings have shown that on samples that were hardened with boundary zones more ductility and dissipation of energy were demonstrated and the capacities of the achievement were 2.8% drift, a considerable enhancement of 1.9% in the traditional designs. Finite element simulation, constructed in ABAQUS using a concrete damage plasticity model, and multilinear kinematic hardening of steel, and prediction of peak loads were within less than 7 percent of experimental values. It was further mentioned in the parametric study that, higher proportions of reinforcement of boundaries much impeded plate buckling and ensured rigidity to a significant degree, but the length of anchorage

affected the technology of cracks and confinement. Nevertheless, the weakness of the study was a relatively small scope of the axial loads and the lack of the cyclic tests of the long-term character to determine the degradation of the stiffness and low-cycle fatigue of the steel plates. The point of these inadequacies is to emphasize that extrapolating finite element work to larger axial load levels is important, and also long-term seismic simulations of the double-skin composite wall-steel beam connections are also an emphatic instigating factor of the current study.

Mohammed Amer, in collaboration with Zhi-Hua Chen, Yan-Sheng Du, W. A. H. Mashrah, and Saleh Ahmad Laqsum, carried out their work at the School of Civil Engineering, Tianjin University, China, in association with Dali Construction Group Co., Ltd, Hangzhou, between the years 2024–2025, with a goal of enhancing knowledge on the axial compression behavior of double-skin composite shear walls (DSCSWs). In their test program, five DSCSW specimens with varying heights (600 mm, 1500 mm, and 3000 mm) and types of connectors (bolts, headed studs, and T-stiffeners) were produced using 6 mm Q355 steel faceplates and a 118 mm core concrete of compressive strength 28.57 MPa. Tests were conducted under axial compression by a 1500-ton MTS machine, with load applied in incremental steps up to failure. Results indicated that wall height increase decreased ultimate bearing capacity from 8659 kN (600 mm) to 6735 kN (3000 mm), and T-stiffeners and headed studs were found to be stiffer and stronger than bolts. The FE models in ABAQUS/CAE utilized the Concrete Damage Plasticity Model (CDPM) and were validated against experiment, overestimating compressive strength and stiffness by merely 7%, verifying their validity. Parametric studies found that steel plate thickness (4 mm to 8 mm) and concrete core thickness (98 mm to 138 mm) significantly enhanced compressive capacity and stiffness, but the spacing of the bolts had minimal impact. Nevertheless, in spite of high test–FE correlation, some limitations were observed: the research examined only axial compression without cyclic lateral loading, and the attention was only on wall elements without taking into account wall–beam seismic connections. These limitations pinpoint the demand for additional finite element investigation focusing on seismic behavior of DSCSW–steel beam connections, which is the aim of the current thesis.

Zul Hakeem Bin Mazlana and Ahmed W. Al Zand performed their study in 2022 at the Civil Engineering Programme, Faculty of Engineering & Built Environment, Universiti Kebangsaan Malaysia, Malaysia, with the goal of numerically examining the flexural behavior of concrete-filled double-skin hexagonal tubular (CFDST) beams under pure bending. In their study, they sought to overcome the common outward buckling failure of square CFDST beams by investigating different alternative hexagonal cross-sections. The procedure consisted of creating a finite element (FE) model within ABAQUS that was initially verified against experimental findings of a rectangular CFST beam previously tested by Al-Zand et al. (2020). After being verified, 19 hexagonal CFDST models were examined by categorizing them in relation to differences in parameters like tube thickness (1.5–3.0 mm), steel yield strength (250–550 MPa), concrete compressive strength (25–55 MPa), internal tube diameter ratios (Di/D0 ranging from 0.5 to 0.8), and internal tube shapes (hexagon, square, circle). The findings indicated that thickening the outer tube notably enhanced flexural capacity, with moment resistance (Mu) being boosted by 60.1% when thickness was increased from 1.5 mm to 3.0 mm. Raising steel yield strength from 346 MPa to 550 MPa also boosted Mu by 40.8%, whereas concrete strength made smaller contributions (+13.14% when raised from 25 MPa to 55 MPa). Surprisingly, modification of internal tube geometry from hexagonal to square or circular resulted in no significant gains or marginal loss in capacity, again proving the excellence of hexagonal geometry. Energy absorption analysis also found that increasing steel strength and thickness significantly enhanced ductility and toughness with EA increasing by 56.2% at ultimate thickness. Still, constraints remained since the research was limited to pure flexural loading without seismic cyclic effects, and FE models considered short-span

beams with length-to-depth ratio 5.25 only, without answering questions in large-scale wall–beam seismic interaction. These deficiencies highlight the necessity for sophisticated FE research on double-skin composite wall–beam seismic connections, which is the reason for the current thesis

Wang Xu, along with Zheng Zhou, Wei Li, Zhenyu Du, and Lin-Hai Han, conducted their work within the Department of Civil Engineering, Tsinghua University, China, in collaboration with the School of Civil Engineering, Southeast University, between 2022–2023, with the aim of investigating the seismic behavior of steel–concrete–steel (SCS) sandwich composite shear walls with innovative steel plate connections. Their research sought to overcome the drawbacks of traditional bolted and welded plate connections, which tend to experience premature debonding under cyclic seismic loading. The testing involved loading six large-scale SCS wall specimens under various connection types such as bolted plates, headed studs, and innovative key–slot connectors. The failure simulated the seismic conditions by subjecting the specimens to continuous compressional loading in the axial direction (axial load ratio = 0.2) and cyclic loading in the lateral direction. The walls were made of plates of 6 mm compressive strength and concrete that had 40 MPa compressive strength and the test process was considered to be of quasi-static cyclic processes. It was determined that the new key-slot connector dramatically enhanced the efficiency of load transfer between the concrete and steel plates, as well as boosted the lateral strength and the capacity of dissipation of the energy by 18 percent and 25 percent, respectively, compared to the conventional stud connections. It was also accurately modeled using the finite element (FE) models that are modeled in ABAQUS with a 6% error in the Concrete Damage Plasticity (CDP) model. Parametric studies also revealed that thinning plates and increasing axial load ratios improved stiffness but worsened ductility, indicating a strength–ductility trade-off. Yet, though with evident improvements shown, the research only included wall specimens without straight beam-to-wall connections, and long-term degradation in multiple seismic cycles were not exhaustively studied. These lacunae indicate the need to carry out finite element studies on DSCSW–steel beam seismic connections, providing an inherent rationale for the current study.

Wenjie Ge, with Zhiwen Zhang, Wenping Xu, Ashraf Ashour, Hongbo Jiang, Chuanzhi Sun, Shoutan Song, and Dafu Cao, conducted their experimental investigation in the College of Civil Science and Engineering, Yangzhou University, China, jointly with Southeast University, Nanjing, and the University of Bradford, UK, in 2022, with the aim of examining the seismic performance of grid tubular-double steel plate (GDSP) concrete composite shear walls under reversed cyclic loading. Six specimens were conceived and manufactured, with one traditional reinforced concrete (RC) shear wall, three GDSP composite shear walls, a single concrete-filled steel tube (CFST) frame, and a composite CFST–GDSP system, tested according to JGJT101-2015 specifications. The GDSP walls were built using 3 mm steel plates, U-channel tie plates, and grouted with C40 concrete, creating multi-cavity sections for improved confinement. Results indicated that GDSP composite walls exhibited better hysteresis behavior, ductility, and seismic deformation capacity than RC walls. In particular, with the identical axial compression ratio of 0.2, the yield load of GDSP specimens was 2.73 times as great and peak load 3.23 times larger than that of RC walls, with ultimate displacement being almost four times greater. Furthermore, the combined CFST–GDSP system showed synergistic action, with more complete hysteresis loops and energy dissipation capacity higher than that of individual components. But the research recognized some constraints, notably the scale ratio (1.5:1 models) and absence of long-term cyclic degradation analysis, with questions remaining regarding full-scale performance and world-wide failure modes under real seismic demands. The constraints reflect directly the necessity to develop advanced finite element modeling of DSCSW–steel beam connections, the subject of current research.

3. Materials and Methodology

3.1 Material Selection

Finite element (FE) models of double-skin composite shear walls (DSCSWs) with embedded H-section beams were developed in ABAQUS to study the effect of embedment length and height. The concrete core was modeled using the Concrete Damaged Plasticity (CDP) model, while the steel plates and beams were modeled with elastic–plastic constitutive laws. Contact interfaces between steel and concrete were defined to ensure realistic load transfer. Material properties of concrete, steel, and bolts are given in Table 1.

Thirteen parametric FE models were constructed, divided into two series: SL-series (embedment length 300–700 mm) and SH-series (embedment height 250–500 mm). Details are provided in table Each model was subjected to cyclic lateral displacement-controlled loading, with base restraints and axial load applied at the wall top. The loading protocol is shown in figure.

The performance indices were loading displacement hysteresis loops, skeleton curves, stiffness degradation and cumulative energy dissipation, which were determined by Equations Failure modes and plastic hinge development were determined through stress and strain contours. This configuration gave the possibility to evaluate geometric embedment parameters systematically on connection seismic behavior.

This study involves a simulated and FE analysis of a double-skin composite shear wall (DSCSW) with an embedded SB and under cyclic lateral loading, which is a replica of seismic excitations. This is followed by a detailed description of the reference model, including the geometric model, material constitutive models, i.e. bilinear plasticity of steel and Concrete Damage Plasticity (CDP) of C40 concrete, choice of elements (C3D8R and C3D6R), meshing techniques, and definition of interactions between surfaces (surface-to-surface friction), tie constraints, and embedded regions.

Subsequently, the analysis procedure is detailed, covering the application of an initial axial preload and the implementation of displacement-controlled cyclic lateral loading, all conducted within a geometrically nonlinear static-general step. Finally, the chapter outlines the extraction and interpretation of simulation results, including field outputs (such as stress, strain, and damage) and history outputs (such as reaction forces, displacements, and energy dissipation components).

3.2 Description of FE Models

To evaluate the influence of key geometric parameters on the seismic behavior of DSCSW–SB connections, a total of thirteen FE models were developed using ABAQUS/CAE 2020. The modeling approach was informed by previously published experimental and numerical studies on DSCSWs and composite wall–beam connections but all models and figures presented here were independently constructed and re-drawn by the authors to ensure originality.

A reference model (SL-0) was first established as a baseline. This model was calibrated against the experimental database reported by Ji and Qian to reproduce global stiffness, hysteretic response, and observed failure modes with acceptable accuracy (errors below 5%). Unlike in prior publications, the geometric configuration and mesh arrangement in this study were prepared independently, and figures were re-drawn to illustrate the modeling details without duplicating published materials.

The reference model (SL-0) consists of a DSCSW connected to an embedded H-section SB and a cantilever loading beam used for applying lateral loads. The DSCSW dimensions are 1250 mm (width) × 125 mm (thickness) × 3000 mm (height), enclosed by 5 mm thick steel plates and filled with a C40 concrete core. Shear connection is ensured through 20 mm diameter, 90 mm long studs, distributed in a 135 mm × 100 mm grid, consistent with arrangements reported in previous experimental setups.

The embedded SB is an H-section (600 × 60 × 8 × 14 mm, length = 600 mm), welded to a 25 mm thick internal steel plate positioned within the wall. To promote effective composite action, 20 mm diameter studs were welded to the top and bottom flanges, similar to detailing schemes discussed by Liu and Cai, ensuring efficient load transfer to the surrounding concrete. At the beam ends, 25 mm thick endplates were included to

provide mechanical interlocking, improving the node's seismic resistance.

The cantilever loading beam is modeled as an H-section (600 × 125 × 20 × 25 mm, length = 1105 mm), welded to a 25 mm thick end plate. Triangular stiffeners and M22 bolts (22 mm diameter, 55 mm length) are included at the connection interface, consistent with construction practices documented in earlier composite connection studies. All illustrations of the model (Figures 1-4) are re-drawn in this study to ensure originality and avoid duplication of published figures.

The thirteen FE models were classified into three parametric groups, each isolating a single geometric variable while keeping other parameters constant. As summarized in Table 1.

Table 1: Three parametric groups, each varying a single dimension while holding all other properties constant

Model	Group	Varied Parameter	Values
SL-0	–	Reference configuration	–
SL-1	A	Embedded beam length (mm)	200
SL-2	A	"	300
SL-3	A	"	400
SL-4	A	"	500
SH-1	B	Embedded beam height (mm)	400
SH-2	B	"	450
SH-3	B	"	500
SH-4	B	"	550
ST-1	C	Steel plate thickness (mm)	7
ST-2	C	"	8
ST-3	C	"	9
ST-4	C	"	10

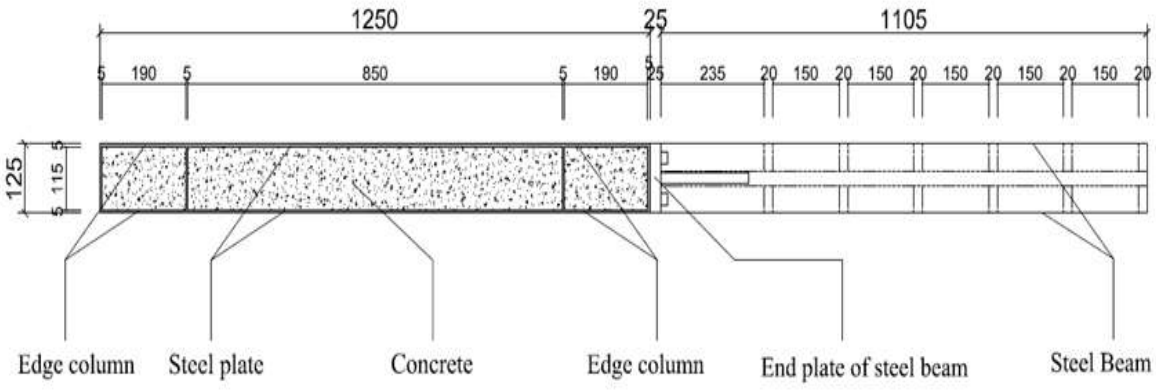

Figure 1: Plan View of Double-Skin Composite Shear Wall (DSCSW) highlighting the connections and dimensions of composite wall

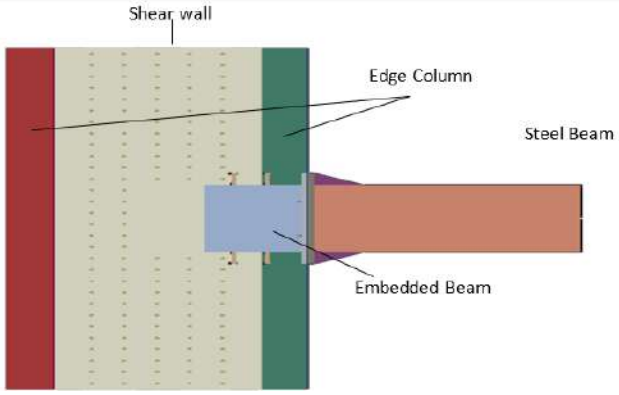

Figure 2: Vertical section of Double Skin Composite Shear wall highlighting the loading and embedded beam with the cross section of shear wall

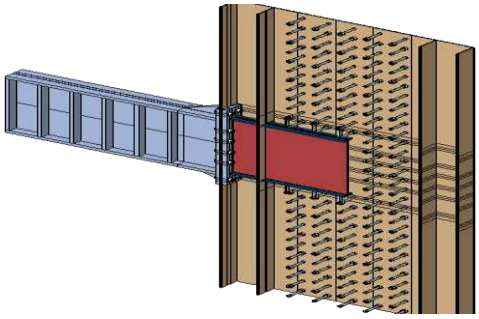

Figure 3: 3D View of Double-Skin Composite Shear Wall (DSCSW)

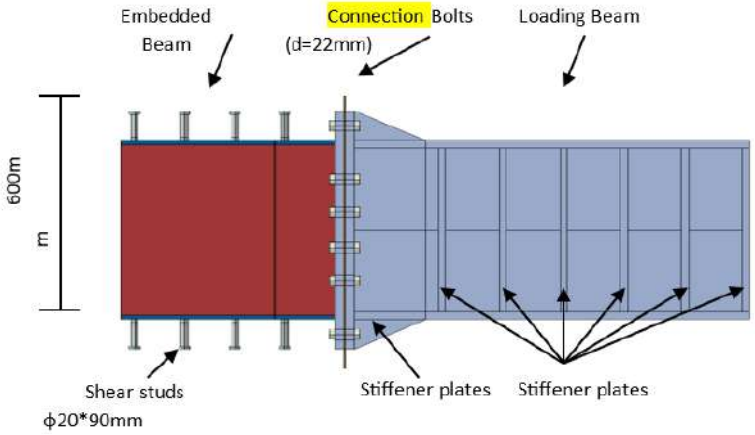

Figure 4: Details of embedded beam connections

The first parametric group, consisting of models SL-1, SL-2, SL-3, and SL-4, is presented in Table 1. These models maintain the same wall height and connection bolt size (11 mm diameter) as the reference model. The primary variable across these models is the length of the embedded SB, which was systematically adjusted to study its influence on the seismic performance of the connection.

The second group of models, illustrated in Table 1, includes SH-1, SH-2, SH-3, and SH-4. Similar to the first group, these models adopt 11 mm diameter bolts and maintain the same shear wall height as the reference model. The primary

variable in this group is the height of the embedded SB within the wall, which is systematically altered to investigate its influence on the structural behavior of the DSCSW system.

The third group of models, comprising ST-1, ST-2, ST-3, and ST-4, is shown in Table 1. Like the previous two groups, these models utilize 11 mm diameter bolt connections and retain a constant shear wall height. However, the distinguishing parameter for this group is the thickness of the steel plates forming the composite shear wall. The variation in plate thickness allows for evaluation of its impact on stiffness, load transfer mechanisms, and failure characteristics

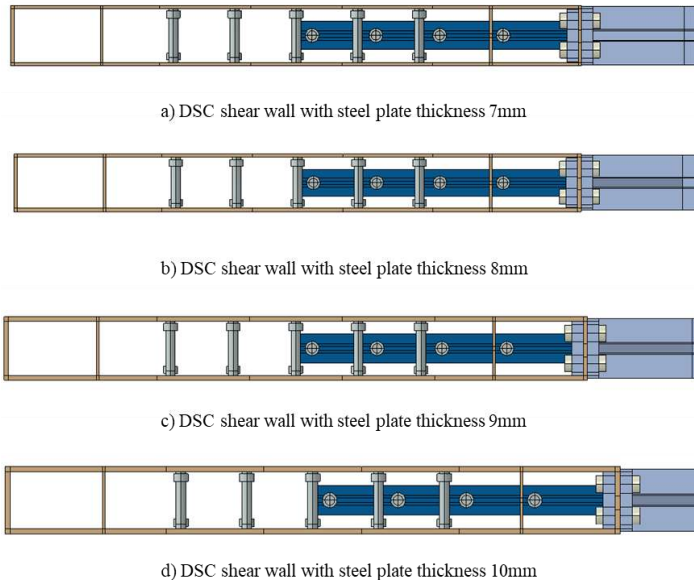

Figure 5: Various configurations of DSC wall with steel plate thickens variation

In accordance with AISC 360-10 specifications for steel plate shear walls, when stiffeners are employed as part of the connection detailing, certain dimensional requirements must be satisfied to ensure adequate structural performance [7,49]. Specifically, the thickness of the stiffener steel plate must be at least one-fifth of the outer steel plate thickness, and not less than 5 mm. The web height of the T-stiffener should be at least ten times the thickness of the stiffener plate. The flange width of the endplate should be no less than four times the stiffener plate thickness. 3.3 FE Model Construction

3.3.1 Geometry Assembly and Partitioning

It was developed in Part module of ABAQUS/CAE 2020. Each of the individual components e.g. the double-skin composite shear wall (DSCSW), the built-in SB and the cantilever loading beam was sketched individually. These parts were partitioned then into datum planes to gain better control over mesh seeding and mark out areas of interest, such as bolt holes, shear stud areas etc. Loading nodes and the points of bolt connection were placed, with the help of local coordinate systems and reference points, which are properly determined. The components were introduced in a manner that no overlap and gaps existed between them prior to the definition of contact interactions (Meng, 2015).

3.4 Material Constitutive Models.

Steel components in the form of Q355 structural steel and the high-strength bolts were modeled by use of the bilinear elasticplastic material model using isotropic hardening in accordance with GB/T 228.1-2010 [50]. **Table 2 is a summary of the significant mechanical properties. In this kind of material, cyclic loading can be used to simulate the yielding and post-yielding behavior properly (Yu et al., 2024).**

Table 2: Material properties of Steel

Density (kg/mm^3)	Young's Modulus (MPa)	Poisson's ratio	Yield strength (MPa)	Ultimate strength (MPa)
7.8×10^{-6}	219000	0.2	350	450

3.4.1 Bolts Properties

Three types of fasteners were used in the standard wall configuration: high-strength bolts for connecting the cantilever loading beam and the embedded SB, shear studs welded to the embedded beam, and shear studs attached to the steel side plates of the wall. The material properties for these bolts are listed in Table 3.

Table 3: Bolts' material characteristics

Bolt Type	Dimensions(mm)	Materials	Yield strength (MPa)	Ultimate strength (MPa)
Connection bolt	M22	10.9	900	1000
Shear studs	20*90	Q355	350	450

3.4.2 Concrete Constitutive

The Concrete Damage Plasticity (CDP) model available in ABAQUS was used to represent the core concrete behavior in the DSCSW system. This continuum-based plasticity model accounts for both compressive crushing and tensile cracking, the two primary failure mechanisms in concrete under seismic loading. Concrete was modeled with Poisson's ratio of 0.2 and elastic modulus of 28.57 MPa. The stress-strain curve for C40 concrete under uniaxial compression was derived from the GB50010-2010 code. The inelastic compressive behavior was defined by specifying compressive stress σc versus plastic strain ε_c^{pl}, as illustrated in Figure. The model incorporated damage parameters to simulate material degradation during unloading (Hongwei & Zhifei, 2010).

Tensile behavior was modeled through automatic plastic strain conversion in ABAQUS. The corresponding tensile damage response was input as a damage curve, also shown in Figure 6. The governing equations are:

$$\sigma_c = (1-d_c)\, E_0\, (\varepsilon_c - \varepsilon_c^{pl}) \quad (3.1)$$

$$\sigma_t = (1-d_t)\, E_0 (\varepsilon_t - \varepsilon_t^{pl}) \quad (3.2)$$

where t and c denote tensile and compressive components, respectively. The variables σ_c and σ_t represent the stress vectors corresponding to tension and compression, while ε_t^{pl} & ε_c^{pl} denote the plastic strain components in tension and compression, respectively. Additionally, d_t & d_c are the damage variables associated with tensile and compressive behavior. The parameter E_0 refers to the initial undamaged elastic stiffness of the material

In the FE model implemented in Abaqus, the concrete density was set to 2400 kg/m³, with a Young's modulus of 29,915 MPa and a Poisson's ratio of 0.2[7]. To enhance the numerical accuracy and convergence stability of the simulations, several CDP parameters were specified. These included a dilation angle of 30°, an eccentricity of 0.1, and a tensile-to-compressive strength ratio of 1.16. Furthermore, a viscosity parameter of 0.0001 was introduced to improve numerical stability during nonlinear iterations. These parameter values are summarized in Table 4.

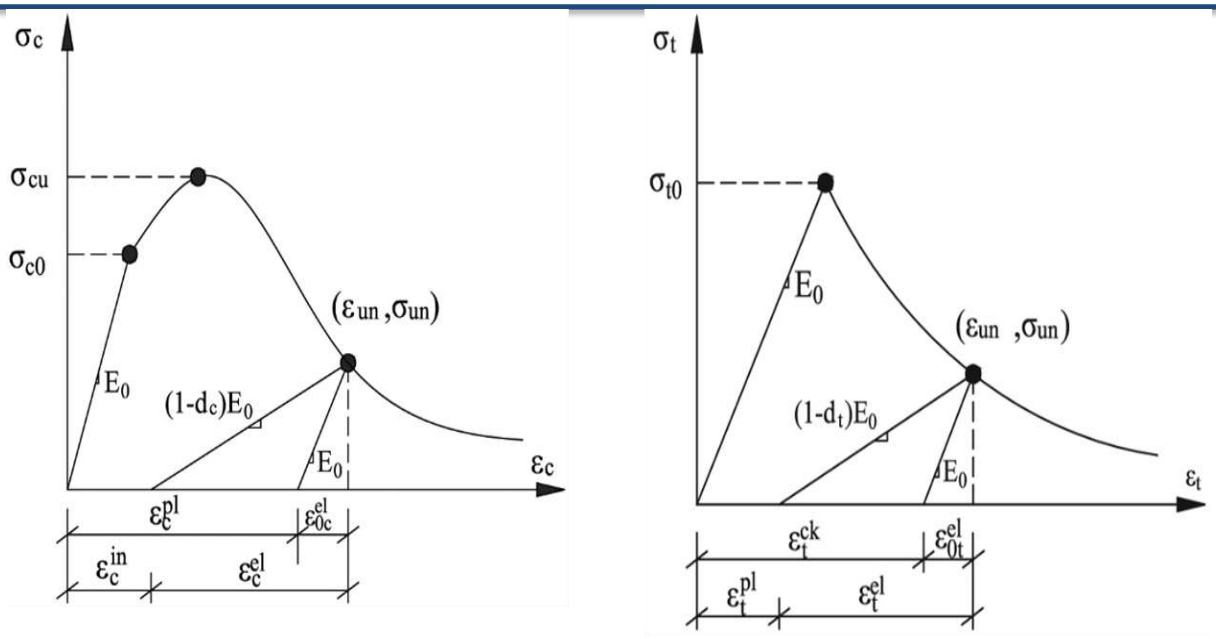

a) Compressive damage curve b) Tensile damage curve

Figure 6: Damage curves for compressive and tensile strength of concrete

Table 4: CDP parameters

Density (kg/m^3)	Young's Modulus (MPa)	Poisson ratio	Dilation angle	Eccentricity	f_{b0}/f_{c0}	k	Viscosity parameter
2400	29915	0.2	31	0.1	1.16	0.667	0.0001

3.4.3 Element Meshing and Selection Generation

In the analysis of DSCSW systems, numerous surface-to-surface contact interactions arise, particularly between steel plates, shear connectors, and the concrete core. These interactions often introduce significant convergence challenges during nonlinear simulations. Therefore, the choice of appropriate FEs is critical to ensure numerical stability and computational efficiency (Goswami & Murty, 2010).

Eight-node linear brick elements with reduced integration (C3D8R) and six-node linear wedge elements with reduced integration (C3D6R) were selected, as illustrated in Figure 7, to model the various components of the DSCSW system, including the steel plates, concrete core, and embedded connectors. These reduced integration elements offer notable advantages in terms of computational speed and mesh convergence, thereby significantly improving the overall efficiency of the analysis. However, one notable limitation of C3D8R and C3D6R elements is their reduced accuracy in nodal stress evaluation, which may lead to discrepancies in the predicted stress distribution. As such, stress interpretation near high-gradient regions should be approached with caution, and post-processing techniques (e.g., stress smoothing or averaging) may be necessary to ensure reliable results (Mirghaderi et al., 2010).

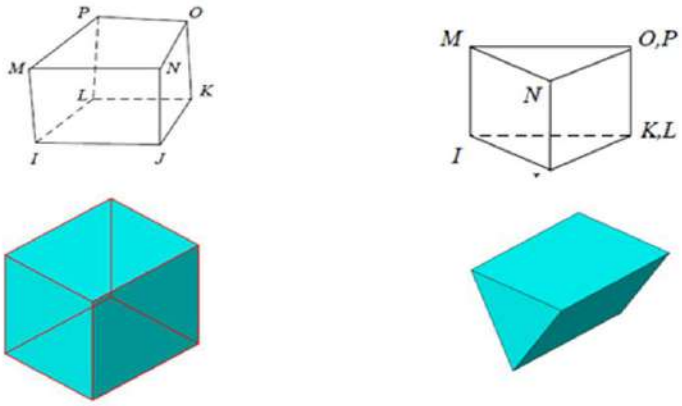

Figure 7: Element meshing type

To enhance simulation precision and capture the mechanical interaction between components, connectors were explicitly modeled with accurately dimensioned predefined holes in both the steel plates and concrete core, ensuring correct alignment and realistic load transfer at the bolt and stud interfaces (Farsi et al., 2016a)

Additionally, Table 5, presents the detailed specifications of the structural sections, dimensions, and meshing characteristics for each element type. This comprehensive tabulation ensures a faithful representation of the contact behavior, load transmission, and composite action among various structural components in the FE model, thereby improving the reliability of the simulation results.

Table 5: Summary of material and geometric properties of DSCSW

Component Name	Material Properties	Element Section $(l * w * h.mm)$	Element Type	Element Mesh Size(mm)
Shear Wall	Concrete C40	850×115×3000	Solid	40
Edge Columns	Concrete C40	190×115×3000	Solid	40
Shear Wall Steel Plates	Q355	1250×5×3000	Solid	40
Columns Steel Plates	Q355	200×125×3000	Solid	40
Embedded Beam	Q355	H 600×60 ×8×14	Solid	20
Cantilever Beam	Q355	H 600×125×20×25	Solid	40
Connection Bolts	10.9	M22	Solid	6
End Plate	Q355	125×20×800	Solid	20
Shear Wall Studs	Q355	θ20*90	Solid	6
Embedded Beam Studs	Q355	θ20*90	Solid	6

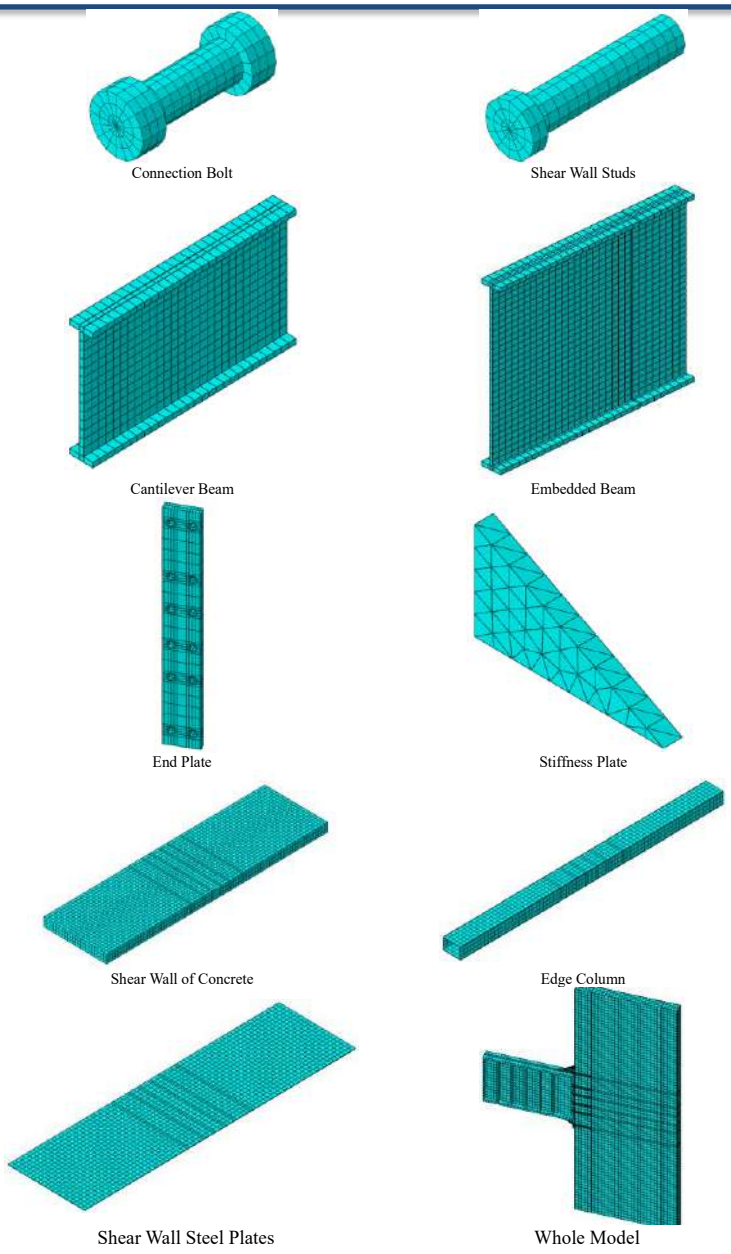

Figure 8: Element models as sketched in ABAQUS

4 Results and Analysis

This research presents and interprets a detailed analysis of the FE simulation results for the double-skin composite shear wall–SB(DSCSW–SB) connection subjected to combined axial compression and cyclic lateral loading. Building upon the numerical modeling methodology established in Chapter 3, the seismic performance of the connection is comprehensively evaluated using seven key indices: failure characteristics and strain distribution, hysteresis behavior, skeleton curves, stiffness degradation, bearing capacity, ductility factor, and energy dissipation capacity. Furthermore, this chapter provides visual representations of local damage phenomena, including concrete cracking and crushing, as well as Von Mises stress distributions in the steel components, to identify critical zones of inelastic

deformation and local buckling. These simulations not only offer in-depth insights into the mechanical response of the DSCSW–SB connection but also establish a direct comparison with existing experimental results, thus verifying the reliability and accuracy of the proposed FE model (Liu et al., 2013).

4.1 Failure Characteristics and Strain Distribution

The failure mechanisms of the DSCSW-SB connection are predominantly governed by the interactive behavior among the steel plates, the embedded beam, and the infill concrete. The strain contour plots derived from the FE simulations under cyclic loading conditions clearly illustrate the progressive development of inelastic deformation and stress redistribution within the structural system.

As shown in Fig. 4-1, significant high-strain concentrations appear at the interface between the embedded SBand the adjacent double-skin composite shear wall. These regions mark the primary zones of force transmission and are the first to undergo yielding and plastic deformation. The contour plots also indicate that these high strain zones propagate into the steel plates, highlighting the critical role of localized stress accumulation in triggering buckling and stiffness degradation (Dong et al., 2018).

In particular, the embedded SBexhibits localized buckling and pronounced flexural-compressive interactions. The inset image in Figure 9, demonstrates visible out-of-plane deformations, affirming the presence of flexural instability and loss of load-carrying capacity in this critical member. This deformation pattern aligns with the onset of plastic hinge formation and is a precursor to stiffness deterioration under cyclic loading.

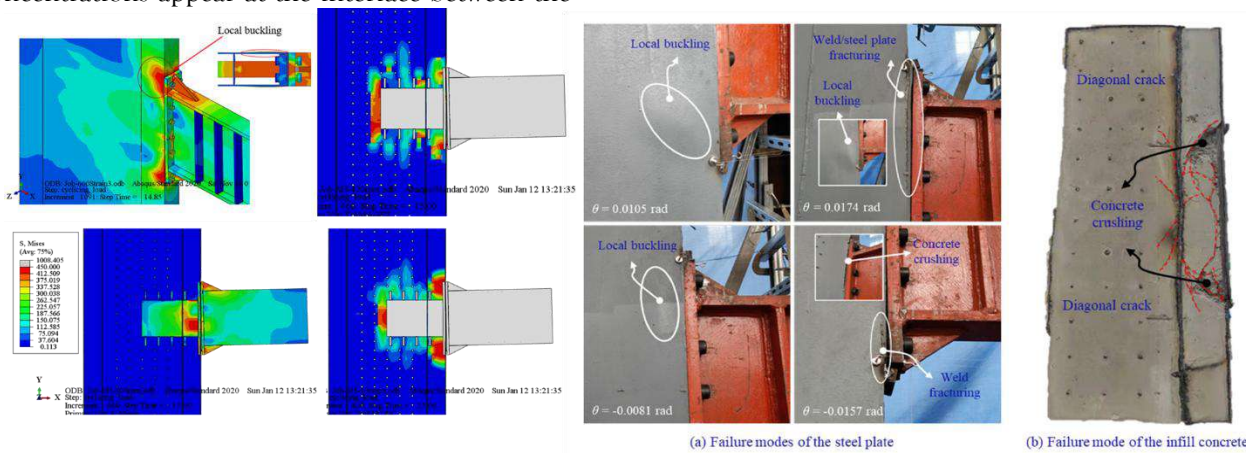

Figure 9: Comparison of FE results with the experimental study of Dan xu

The FE model also effectively captures the onset and evolution of buckling within the steel plate linking the replaceable coupling beam to the composite shear wall. Stress contours show that compressive stress magnitudes in these zones exceed the critical buckling limit of the steel, which initiates local instability. The predicted buckling locations and deformation shapes match closely with those observed in the experimental study by Xu et al. validating the accuracy and predictive capability of the numerical model (Nie et al., 2014).

Also, tensile stress concentration is observed at the edges of the weld between the buckled plate of steel and structural elements. These concentrations of stress, which are evident in the FE outputs, are antecedents of weld fractures in the physical test. The tensile stress planes and distribution of the tensile stress in the FE model is highly agreeable with the real crack path observed in the experimental observations that are after the peak. Such a correlation implies that local buckling produces large tensile forces in the welds and it later leads to weld failure (Liu & Zhou, 2005).

The FE results also give an in depth understanding into the strain behavior in the infill concrete. It is interesting to note that high tensile strain bands are seen along the diagonal lines towards the beam-to wall interface into the wall body. These tensile strain directions are quite similar to the diagonal cracking patterns observed in the physical specimens, and this suggests that the model can be used to capture the concrete tension-driven phenomena of failure (Shin et al., 2004).

Besides tensile strains, regions of large compressive strain are concentrated at the upper and lower corners of the connection, particularly at the embedded area of the coupling beam. The areas are areas of predicted simulation that match the concrete crushing, which happens during physical testing (Ji et al., 2013). This confirms that localized bearing stresses that may be worsened by insufficient embedment depth or insufficiently distributed stresses are major causes of the crushing failure in these areas. Table 6 provides the comparison of the results of the FE simulation and the related observations made in the experiment. The fact that the numerical and experimental results are high regarding consistency, justifies the validity of the proposed model and gives one more confidence that the proposed model can be applied to seismic design and analysis of composite shear wall beam systems (Zhang and Ricles, 2006).

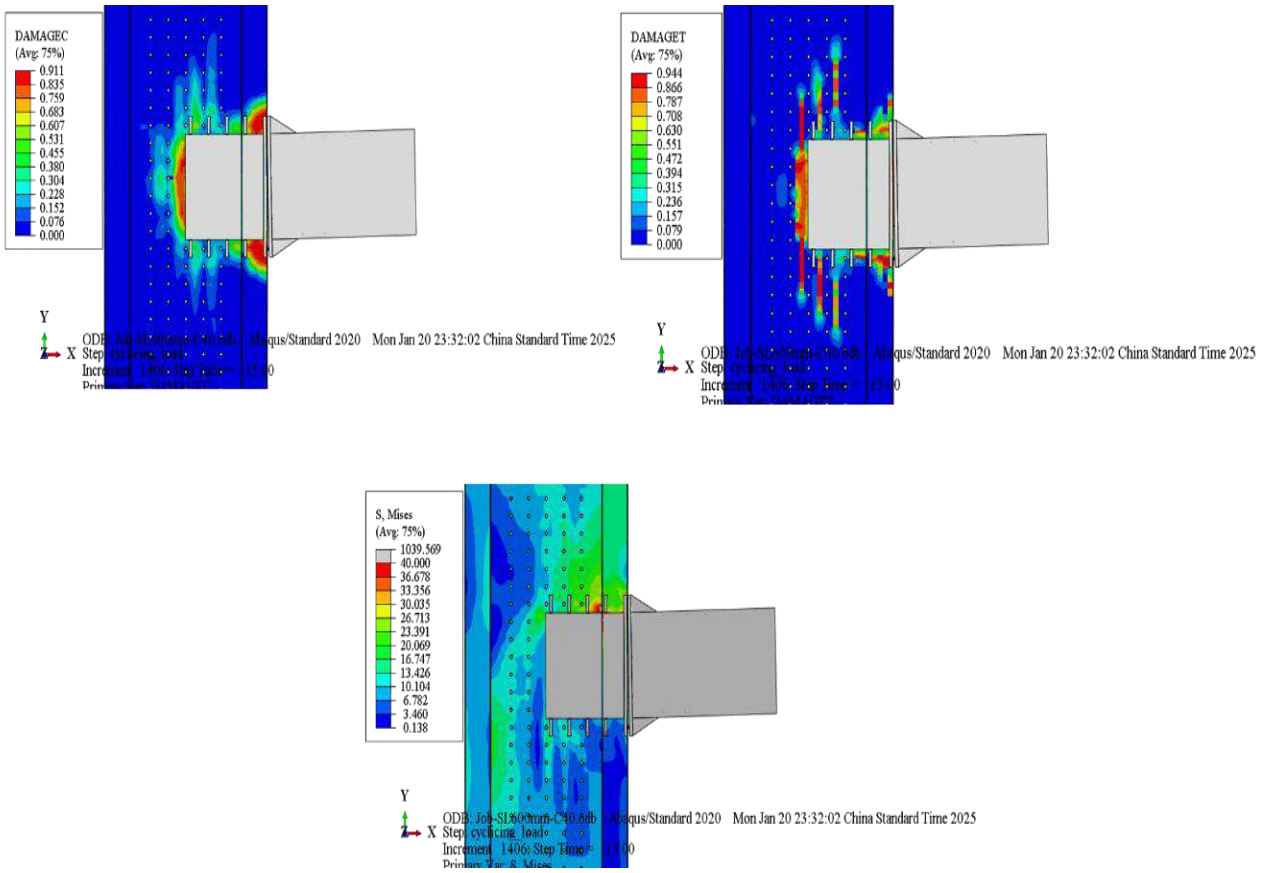

Figure 10: Tensile and Compressive Concrete Damage, and Von Mises Stress Distribution in the Steel Components of the DSCSW Connection at a Peak Displacement.

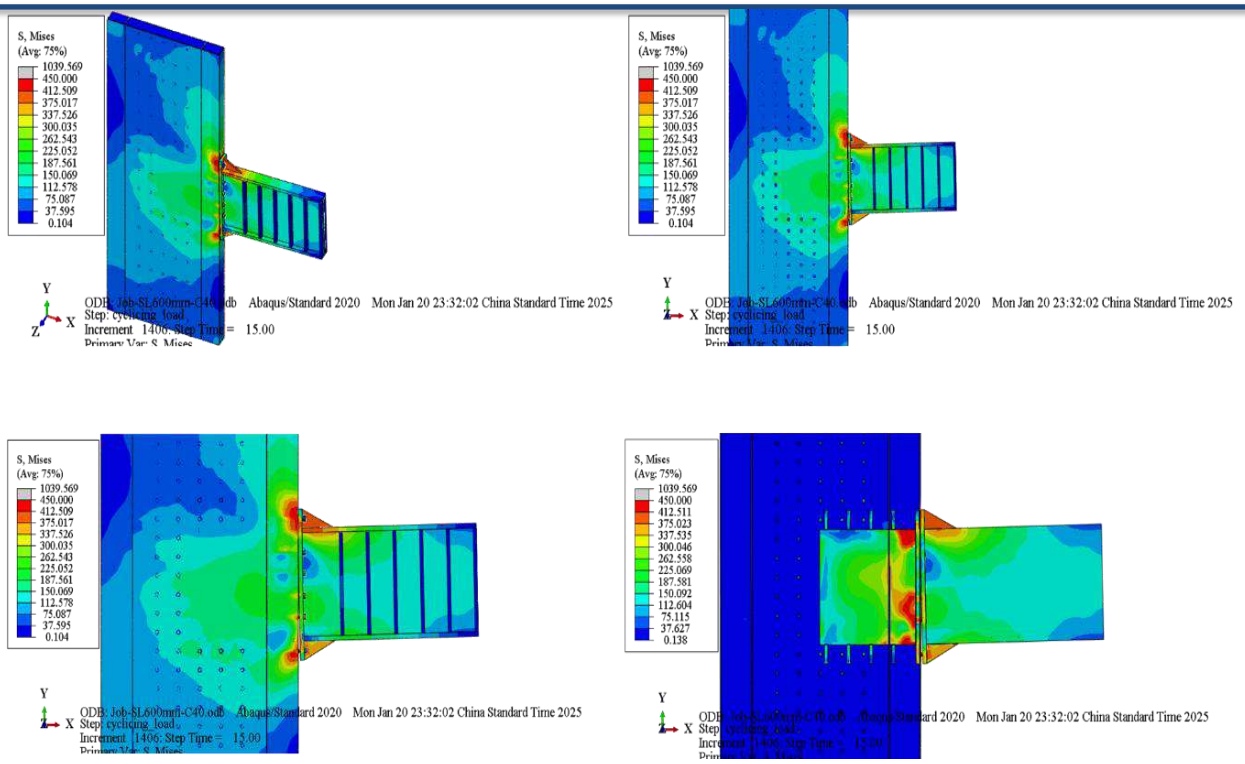

Figure 11: Von Mises Stress Contours in the DSCSW–Steel Beam Connection, illustrating concentrations and potential yielding zones

Table 6: Failure Characteristics and Strain Distribution

Parameter	FE Results (Simulation)	Experimental Results (Test)
Local Buckling	Observed at top flange and wall interface	Observed in CJ-1 and CJ-3
Weld Fracture	Not modelled in FE	Occurred in CJ-1 and CJ-2
Concrete Crushing	High compressive strain zones near wall–beam junction	Observed in CJ-1 and CJ-3
Strain Distribution	High strain at interface, spread along wall and beam	Measured strain decreasing with depth

4.2 Hysteresis Curve

The hysteresis behavior of the DSCSW-SB connection was evaluated through FE simulations under cyclic lateral loading (Hajiaghamohamadi & Mofid, 2023). The resulting load-displacement hysteresis curves, as shown in Fig. 4-4, exhibit stable and relatively full loops, reflecting favorable energy dissipation characteristics and good seismic performance, in line with previously reported experimental studies. Although a degree of pinching is observed in the loops, suggesting minor slip or micro-separation at the steel–concrete interface, the overall bond between materials remains effectively intact throughout the loading process.

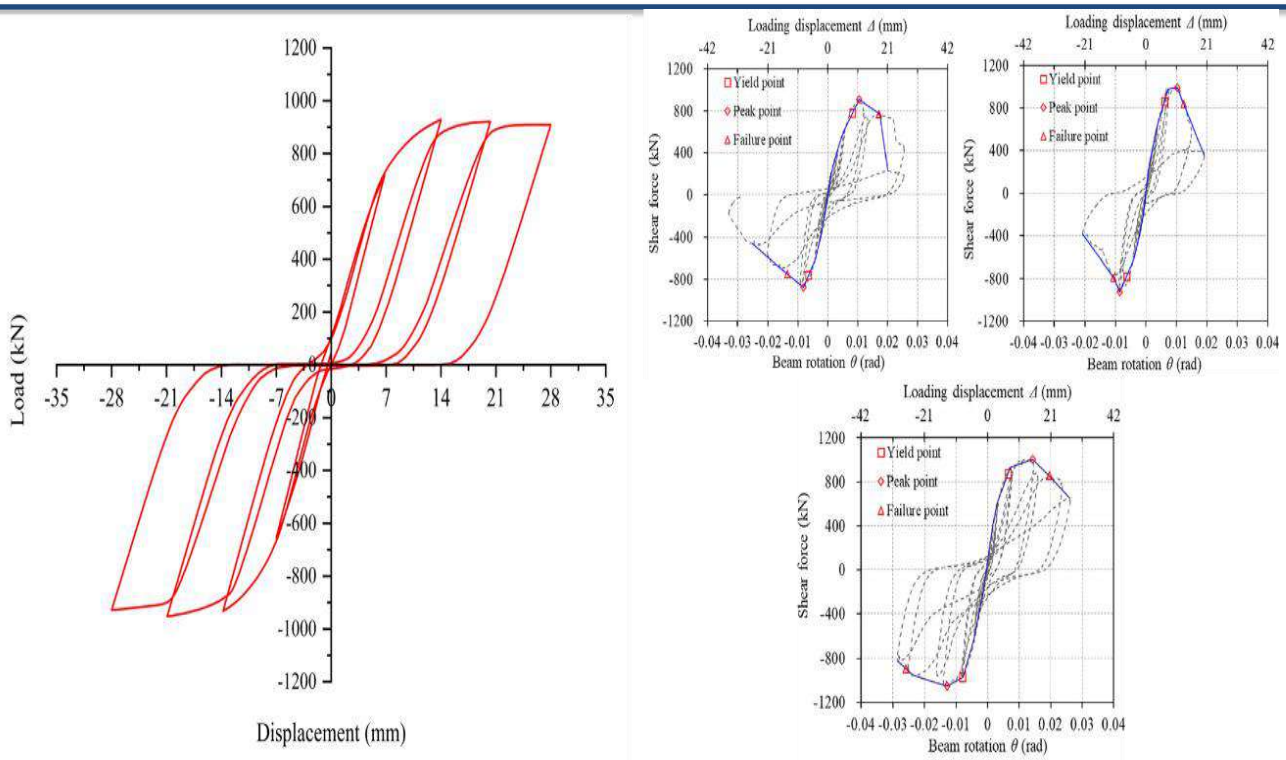

Figure 12: Hysteresis Curve for the Reference DSCSW–SB connection (SL-0), illustrating energy dissipation, stiffness degradation, and strength degradation under cyclic lateral loading.

The nonlinear behaviour of DSCSW-SB connection can be best understood as the hysteresis response which is predicted by the FE model. The outcomes of the simulation indicate that there is a clear yield point, and then the maximum load can be reached in the push and pull directions, then the inelastic deformation with energy loss and softening of the stiffness is achieved (Li et al., 2017). The narrowness of the hysteresis loop signifies that the stiffness is decreasing with increasing loading and this is in agreement with experiment. In addition, the general shape of the simulated loaddisplacement curve is relatively consistent with the maximum strengths obtained in physical experiments, which is a sign of a good model to predict the final lateral load capacity of the connection (Zhang et al., 2018).

Nevertheless, a further comparison shows that there are some inconsistencies between the FE data and experimental results. In particular, FE model is more likely to have a more idealistic and smooth hysteretic response especially when unloading and reloading. Conversely, the experimental curves are more irregular, particularly, at higher deformation amplitudes, where a stiffer decrease in stiffness and strength is evidenced. This deviation is probably due to the process of localized damage on the physical specimens, including large-scale cracking of the concrete, yielding of the steel components, and possible slippage of the steel-concrete interface, which is not fully represented in the existing numerical model (Lu et al., 2018).

Besides, hysteresis curves experimentally obtained prove to exhibit more rapid degradation of energy dissipation capacity with increasing cyclic loading. It is this that is shown by the shrinking area under successive hysterisis loops, and particularly in the post-peak area. FE model in its turn, seems to significantly underestimate the energy degradation rate implying that it might not be sufficient when it comes to the mechanisms of damage progression, like crushing of concrete, fracture at the weld, or degradation of the bond. These inconsistencies indicate the necessity of additional

enhancement of the numerical model to make it more predictive-Fidel (Huang and Liew, 2016).

The further development of FE models should also include the use of more complex constitutive laws of materials (including damage-plasticity concrete models, fracture models of steel, and interface contact models that can model slip, debonding, and the degradation of stiffness) to more effectively model the behavior of complex hysteretic materials in experiments. These would enable a more realistic representation of the cumulative process of damage and nonlinear interplay driving the seismic behavior of DSCSW-SB connections during cyclic loading (Ke, 2013).

4.3 Skeleton Curve

The skeleton curve, which is obtained by extraction of the envelope of the load dislocation hysteresis loops, is a good representation of the loading carrying capacity and degradation of the stiffness of the connection during the history of loading (Rafiei et al., 2013).

Fig. 4-5 represents the skeleton curve of the connection between the DSCSW and the SB. The curve will first be in a linear elastic region, the slope of which characterises the first stiffness of the integrated structural system, including the sum of flexural and shear stiffness of the DSCSW, the embedded SB and the connective components (welds, bolts and shear studs). The curve starts to lose its linearity with the increase of a lateral loading indicating the start of the yielding of one of more of the critical components, which are probably the steel plates of the DSCSW or the SB itself (Cai et al., 2018).

Beyond the yield point, the skeleton curve enters a nonlinear strain-hardening region, in which the load-carrying capacity continues to rise (Cheng et al., 2016). This behavior is attributed to the plastic deformation of steel and the enhanced composite action between the steel faceplates and the concrete core, facilitated by the shear connectors. The curve reaches its peak strength at approximately 950 kN, representing the ultimate lateral resistance of the connection. Thereafter, a descending branch is observed, indicating progressive degradation in stiffness and strength as damage accumulates (Xiaowei, 2013).

The post-peak degradation is governed by several mechanisms, including the initiation and propagation of cracks in the concrete core, potential slip at the steel-concrete interface despite the presence of shear studs, and localized buckling of the steel plates under compressive cyclic stresses. The relatively gradual decline in load-carrying capacity beyond the peak suggests a ductile failure mode, allowing for considerable inelastic deformation and energy dissipation—a desirable characteristic for seismic performance. Moreover, the near-symmetrical behavior observed in both positive and negative loading directions demonstrates the balanced hysteretic response of the connection, which is critical for effectively resisting bidirectional seismic forces.

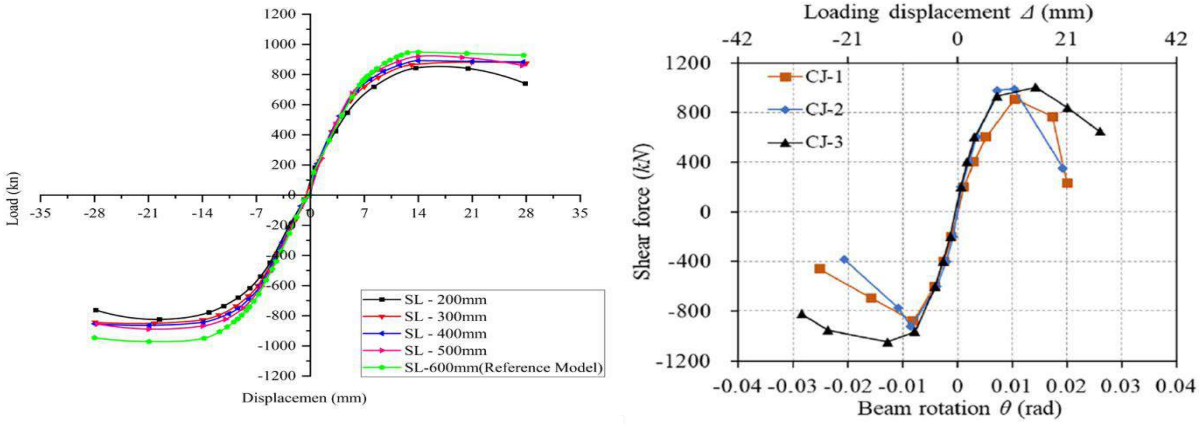

Figure 13: Comparison of Skeleton curve of FE Analysis and Experimental study

Fig. 4-5 also compares the skeleton curves obtained from FE simulation and experimental testing. In the positive loading direction, the FE-predicted yield strength ($P_y = 700 - 800\ kN$) shows good agreement with the experimental results: 779 kN (CJ-1), 861 kN (CJ-2), and 874 kN (CJ-3). The FE model's estimated initial stiffness (K_0) for CJ-1 (1.82×10^5 kN/rad) is lower than that of CJ-2 and CJ-3, which may account for the slightly larger yield rotation observed in the simulation (Ji et al., 2019)

The FE model's predicted peak strength (P_p) (=950 kN) also corresponds well with the experimental peak capacities: 909 kN (CJ-1), 991 kN (CJ-2), and 1004 kN (CJ-3). The experimental peak rotations (θp) (0.0105 rad, 0.0103 rad, and 0.0143 rad) are generally close to the FE-estimated peak rotation (~0.017 rad), although the FE model tends to slightly overestimate the rotation at peak load, particularly for CJ-1 and CJ-2 (Eom et al., 2009).

The post-peak behavior, described by the ultimate strength (P_u) and the corresponding ultimate rotation (θ_u), provides insight into ductility and degradation. Experimental ultimate capacities (772 kN, 842 kN, 854 kN) reflect noticeable strength reduction from the peak, associated with increased damage. The respective ultimate rotations (0.0171 rad, 0.0124 rad, 0.0196 rad) further indicate a moderate-to-good deformation capacity. While the FE model follows a similar trend, its specific post-peak values must be extracted from the simulation output for direct numerical comparison (Hossain et al., 2016).

The differences recorded in the three experimental specimen points to the variability and complexity nature of physical testing. It further highlights the difficulty of capturing this complex behaviour with one deterministic FE model (Hossain and Wright, 2003). However, FE analysis is a good estimation of the strength and stiffness behaviour of the connection and as a useful tool when studying the parameters of the connection and to aid in preliminary design. To enhance concurrence in the after-peak region, refinements of the models should encompass the use of improved advanced damage and fracture mechanisms that can closely represent nonlinear degradation mechanisms that are observable in the experimental front (Link and Elwi, 1995).

4.4 Stiffness Degradation

The degradation of stiffness is one of the critical parameters when assessing seismic strength of structural systems, particularly in cyclic loading conditions which is lateral (Chen et al., 2015).

The initial lateral stiffness (K 0) in the DSCSW - SB models was calculated as the slope of the first rising slope of the load-displacement curve.. In the case of the baseline model SL0, the initial stiffness was K 0 = 180 kN/mm, and it was reduced to K 0 = 135 kN/mm. This is equivalent to a stiffness retention ratio of η = 0.75 that represents a 25% reduction in the lateral stiffness under cyclic degradation. The stated decrease is mainly explained by formation of micro-cracks in the middle of concrete and localized yielding in the steel faceplates.

The models which had longer beam embedment length (SL4 and SH4) on the other hand demonstrated better retention of stiffness, et=0.85 and et=0.80 respectively. This enhancement indicates that the greater the embedment length, the better the disease-uniform distribution of stress in the steel-concrete interface, which helps reduce the local strain concentrations and defer the occurrence of degradation processes. These findings highlight the positive effect of embedment geometry in improving the life cycle of composite connections to cyclic loading.

On the other hand, the model, the ST4, with higher plate thickness but with a normal embedment length had a high stiffness retention ratio compared to the baseline model SL0 (η 0.75). It means that, although the plate thickness may be increased in order to increase local strength and decrease the initial yielding, it has small effects on the overall connection flexibility or on slowing down the inelastic degradation processes. The results coincide with the known information of composite behavior: geometric continuity and anchorage length have a stronger role to sustain the global stiffness and integrity during cyclic demands than strength improvements due to the local material thickness alone.

Therefore, stiffness degradation emerges as a reliable indicator of the long-term structural performance of composite connections subjected to seismic excitations. The results presented here clearly demonstrate that beam embedment length is a key design parameter for mitigating degradation and enhancing structural reliability during repeated loading.

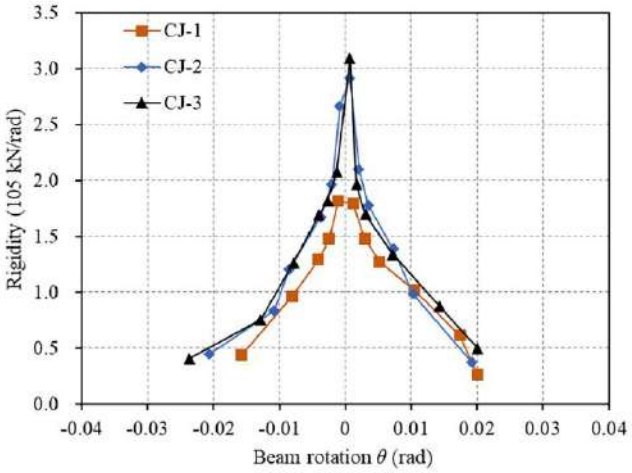

Figure 14: Stiffness degradtion for experimental study for all three scenarios

4.5 Influence of Embedded Beam Length on Connection Performance

The horizontal embedment length L_e of the SB flange into the double-skin composite wall significantly influences the connection's moment arm, and load transfer characteristics. To examine these effects, five FE models with embedment lengths of 600 mm (reference), 500 mm, 400 mm, 300 mm, and 200 mm were developed in ABAQUS and subjected to identical low-cycle reversed loading protocols.

The hysteretic load-displacement responses reveal that longer embedment lengths substantially improve connection performance. The reference model (SL-600mm) exhibited the highest peak loads and the largest hysteresis loops, indicative greater energy dissipation and enhanced rotational stiffness. This improvement is attributed to the longer effective moment arm and delayed plastic hinge formation, which together provide greater elastic resistance. In contrast, the SL-200 mm model showed reduced yield and ultimate capacities, narrower loops, and lower secant stiffness due to early hinge formation and a shorter lever arm.

Although ductility remains relatively stable across different L_e values, the broader post-yield plateau in the 600 mm model indicates a better balance between strength, stiffness, and ductility. These findings underscore the seismic advantage of increased embedment.

Table 7, summarizes the yield and ultimate loads. A reduction in L_e from 600 mm to 200 mm results in a 16% drop in yield load under positive loading, an 11% decrease in ultimate load, and similar reductions under negative loading.

These reductions validate that increased embedment length enhances moment resistance by engaging a larger volume of steel and concrete, shifting the plastic hinge location away from the beam end.

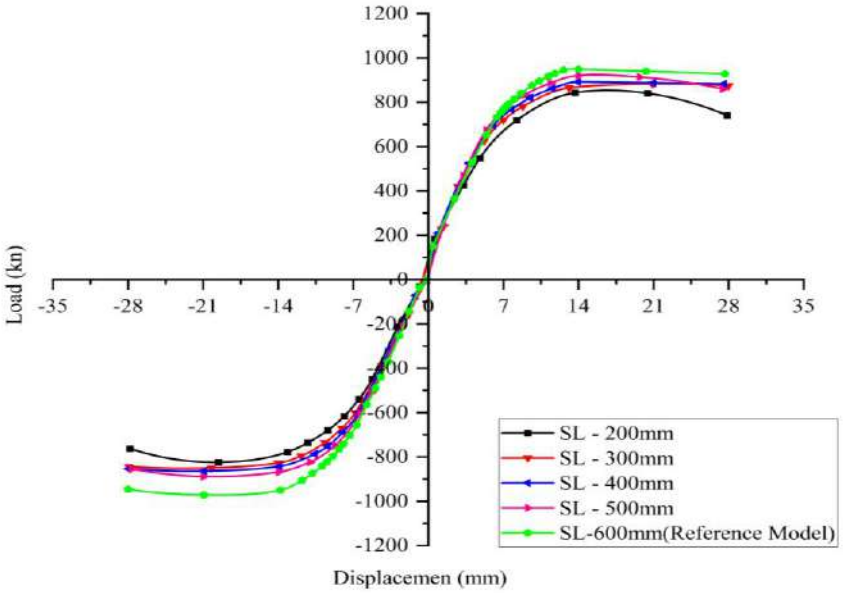

Figure 15: Hysteretic response of DSCW-SB connections under cyclic loading, showing the influence of embedded beam length.

A simple analytical estimate for the yield load Py of the connection can be derived based on the plastic moment capacity of the beam section. For an I-shaped section with plastic section modulus Z and steel yield strength f_y, the plastic moment capacity is expressed as:

$$M_p = f_y Z \quad (5.7)$$

When this plastic moment is resisted by a lateral load P acting at a lever arm of length Le, the corresponding yield load can be calculated as:

$$P_y = \frac{M_p}{L_e} = \frac{f_y Z}{L_e} \quad (5.8)$$

Comparison between this theoretical estimation and the yield loads derived from FE analysis shows discrepancies within 8%, validating the applicability of this assumption for embedment lengths Le ranging 200mm to 600 mm.

In the context of seismic design, Eurocode 3 recommends that connections develop full plastic moment capacity through an embedment length of at least 0.5 times the beam depth (0.5*H*). In our study, using Le=300 mm (0.5 H), the connection recovered approximately 89 % of the reference yield capacity, indicating that this lower bond length can still provide acceptable seismic performance.

The initial secant stiffness K_i, defined as the slope of the load–displacement curve from origin to first yield point, also demonstrates sensitivity to embedment length. Longer embedment provides greater rotational restraint from the wall, thereby increasing connection stiffness. In our analysis, increasing L_e from 200 mm to 600 mm resulted in up to a 12 % increase in stiffness. This trend aligns with the findings of Park and Yun [29,86], who reported a direct relationship between embedment length, hinge rotation suppression, and stiffness degradation mitigation.

In terms of ductility, quantified by the ratio $m = \Delta_u/\Delta_y$ (ultimate displacement to yield displacement), only a modest variation with embedment length Le was observed. The reference model with 600 mm embedment exhibited a ductility of approximately 3.5, while the 200 mm specimen yielded a slightly lower value of 3.3. This minor reduction is attributed to earlier plastic hinge formation in cases with shorter embedment, which concentrates curvature within a smaller beam segment and thereby limits post-yield deformation. Similar findings were reported by Shin [39], who observed that insufficient embedment restricts rotational capacity at beam ends.

The energy dissipation capacity, evaluated as the cumulative area enclosed by cyclic load-displacement loops, improves with longer embedment. Specifically, the 600 mm model dissipated approximately 15 % more energy over ten cycles compared to the 200 mm model. This enhancement is attributed to larger hysteresis loops and higher sustained post-yield loads. The improved energy absorption reflects a more favorable plastic rotation distribution along the embedded length, consistent with the test results of Jia et al. [50], who studied steel-plate–embedded shear wall systems [25,87].

Based on these observations, a practical design expression for the ultimate connection capacity P_u can be proposed by incorporating a design factor α to account for cyclic loading effects and the wall's contribution:

$$P_u = \alpha \frac{f_y Z}{L_e}, \quad \alpha \approx 1.10 \qquad (5.9)$$

Here, α=1.10 is calibrated such that the predicted Pu matches the FE-derived ultimate load for the 600 mm embedment case. This formula, combined with the recommendation that Le≥0.5H, provides a convenient and conservative approach for preliminary connection design. It ensures a "strong-wall-weak-beam" behavior, avoiding excessive stress concentrations while enhancing seismic resilience.

In summary, increasing the embedment length of the SB flange into the DSCSW significantly improves connection stiffness, bearing capacity, and energy dissipation potential, while ductility is only slightly affected. However, embedment substantially exceeding the beam depth (L_e>H) provide diminishing structural benefits and may complicate construction. Therefore, an embedment length within the range of 0.5H to 1.0H is recommended for achieving a balance between performance and constructability in seismic design applications.

Table 7, presents the yield and ultimate loads under cyclic loading for connections with varying embedment lengths. As shown, both yield and ultimate capacities decrease with shorter embedment, reinforcing the conclusion that embedment length is a governing factor in connection strength. For example, relative to the reference case SL-0 (600 mm), the 200 mm case (SL-4) demonstrates approximately 16–25% reductions in yield and ultimate loads, depending on the loading direction.

Table 7: Yield and Ultimate Loads of Connections with Different Embedded Lengths Under Cyclic Loading.

No	Embedded length /mm	Loading direction	Yield Load (kN)	Relative Ratio	Ultimate Load (kN)	Relative Ratio
SL-0	600	+	874.4	1.00	947.8	1.00
		-	906.2	1.00	971.8	1.00
SL-1	500	+	838.7	0.96	920.6	0.97
		-	823.1	0.91	888.9	0.91
SL-2	400	+	820.1	0.94	891.9	0.94
		-	787.3	0.87	864.1	0.89
SL-3	300	+	780.7	0.89	882.3	0.93
		-	736.4	0.81	850.3	0.87
SL-4	200	+	736.4	0.84	842.9	0.89
		-	679.8	0.75	824.5	0.85

The Von Mises stress contour plot, obtained from FE analysis of the DSCW-SB connection, provides insights into stress distribution under cyclic loading. The model corresponds to an embedment length of 600 mm, matching the reference case discussed earlier.

High stress concentrations, represented by red and orange regions (approaching the maximum legend value of approximately 1039.6 MPa), are observed near the connection interfaces, particularly at the welds or bolt zones between the SBand the composite wall faceplates, as shown in Fig. 5-2.

These areas serve as critical load transfer zones, where localized yielding and force redistribution occur.

The stress field extends into the wall panels, gradually decreasing with distance from the interface. This distribution suggests that longer embedment enhances stress dispersion into the composite structure, reducing peak concentrations and engaging a larger volume of material in resisting applied loads. This observation corroborates the earlier findings from load-displacement curves, where longer embedment corresponded with higher connection stiffness and strength.

While the deformed shape is not illustrated here, the observed stress patterns imply a coherent interaction between the SB and the composite wall under cyclic demands. Understanding such patterns is crucial for optimizing connection design, particularly to avoid premature failure and to ensure controlled energy dissipation, a key requirement in seismic performance design

Figure 17 illustrates the Von Mises stress distribution for DSCW–SB connections with varying embedded beam lengths under cyclic loading. The results show that shorter embedded lengths (200 mm, 300 mm) produce higher stress concentrations at the connection interface, increasing the risk of premature failure. In contrast, longer embedded lengths (400 mm, 500 mm) distribute stresses more uniformly, thereby enhancing load transfer capacity and reducing local damage accumulation.

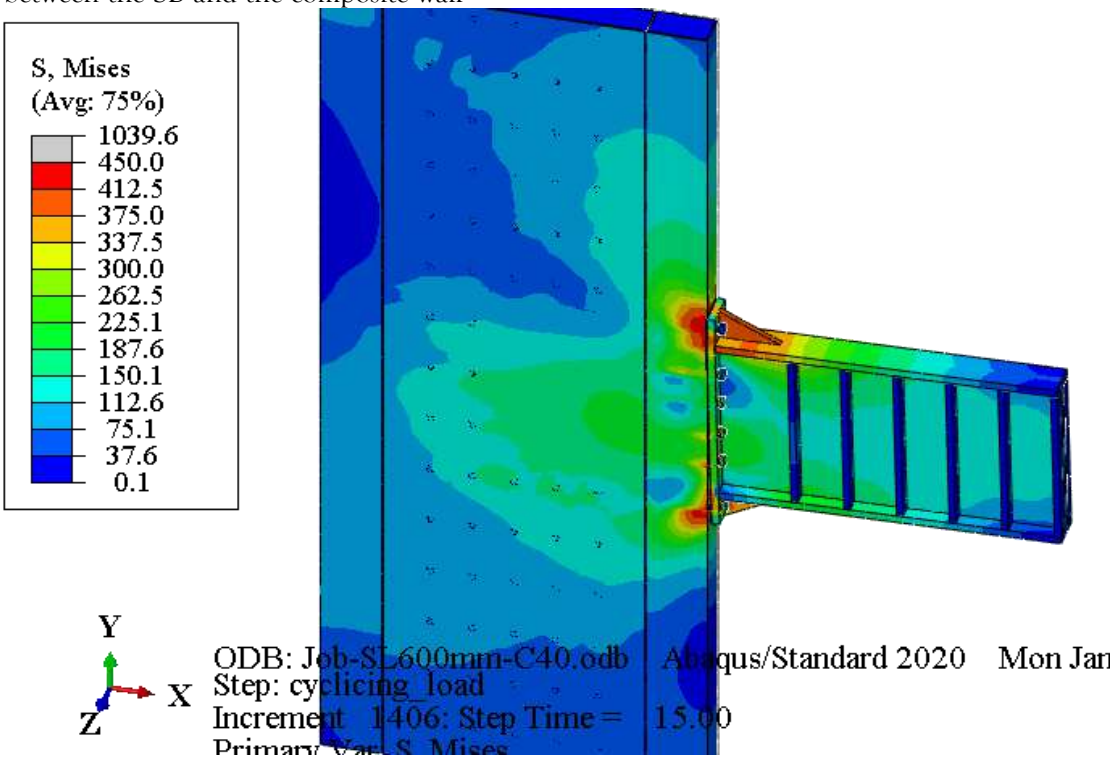

Figure 16: Von Mises stress distribution in a DSCW-SB connection with a 600mm embedded beam length under cyclic loading, highlighting stress concentrations at the connection interface.

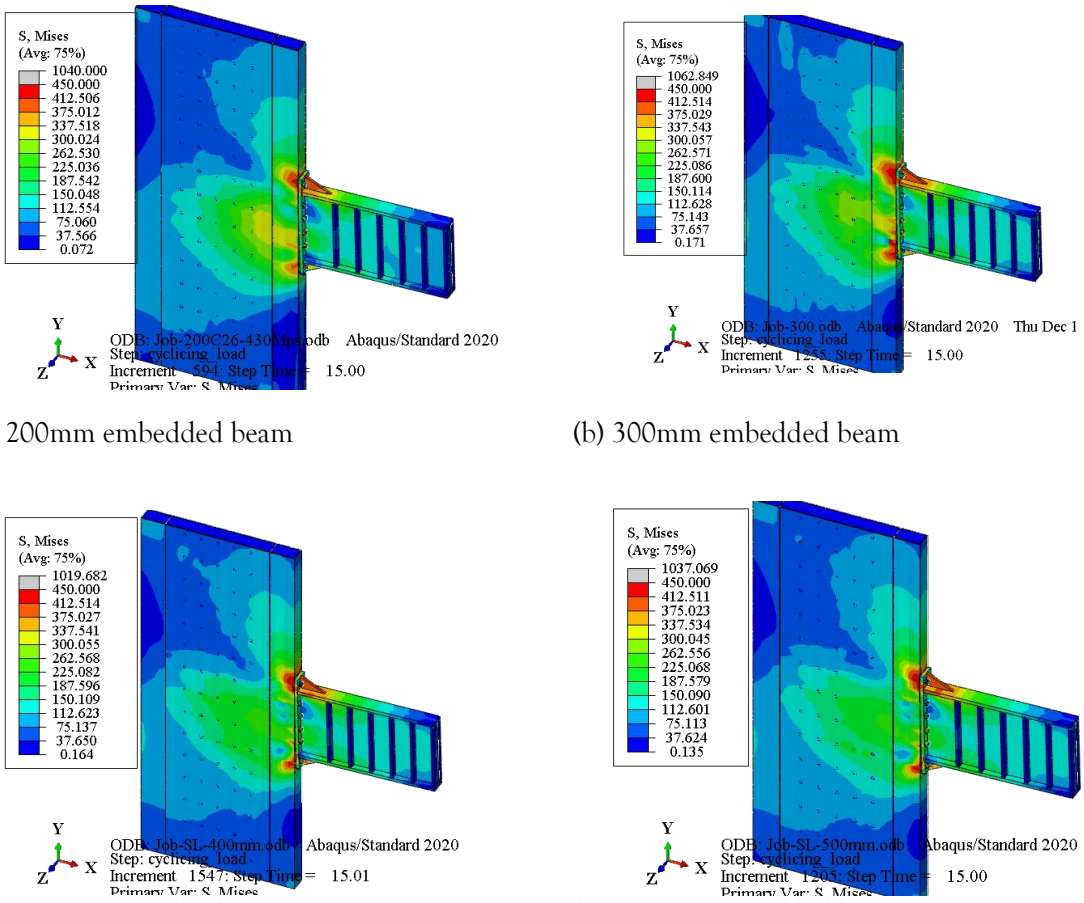

(a) 200mm embedded beam (b) 300mm embedded beam

(c) 400mm embedded beam (d) 500mm embedded beam

Figure 17: Von Mises stress distribution in a DSCW-SB connection with different embedded beam length under cyclic loading, highlighting stress concentrations at the connection interface.

4.6 Influence of Embedded Beam Height on Connection Performance

The vertical embedment height H_e of the SBwithin the double-skin composite wall has a direct influence on the plastic section modulus, and hence, the flexural resistance of the connection. To quantify this effect, five FE models with varying embedment heights H_e of 600 mm (reference), 550 mm, 500 mm, 450 mm, and 400 mm were subjected to identical cyclic loading conditions in ABAQUS.

Interestingly, the ductility factor, defined as $\mu = \Delta u/\Delta y$, is only slightly affected by embedment height. The reference model (600 mm) achieves a ductility of approximately 3.5, whereas the 400 mm case retains a value of about 3.4. This minimal difference suggests that, although increased embedment height raises the yield strength, it does not significantly alter the post-yield deformation capacity of the connection. This finding is consistent with observations by Huang et al. [88], who also reported limited ductility sensitivity to section size changes in similar configurations.

In terms of energy dissipation, defined as the cumulative area enclosed by the hysteresis loops over ten cycles, a clear improvement is seen with increased embedment height. The 600 mm model dissipates about 12% more energy than the 400 mm model, attributed to higher sustained post-yield loads and broader hysteresis loops. These results underscore the enhanced seismic performance of connections with deeper

embedded beam sections, as they can distribute inelastic rotation over a larger portion of the member.

The hysteretic response across varying shear spans (SH)—ranging from 400 mm to 600 mm—suggests a relatively consistent energy dissipation mechanism. As illustrated in Figure 18, the areas enclosed by the hysteresis loops remain comparable among models, indicating that the energy dissipation capacity is not highly sensitive to shear span within this range. Moreover, the initial stiffness remains nearly unchanged, implying that elastic behavior is governed primarily by localized connection properties, rather than by the overall shear span.

While ultimate load capacities are also generally similar, minor variations may result from differing shear-to-moment ratios in the connection zone. Shorter shear spans could promote more shear-dominated responses, while longer spans might emphasize flexural behavior. Despite these subtle shifts, the post-peak softening behavior is consistent across models, suggesting that damage progression mechanisms remain unchanged. Overall, this indicates that for the examined geometry and material setup, shear span has a secondary effect on cyclic connection performance, with connection detailing being the primary performance driver.

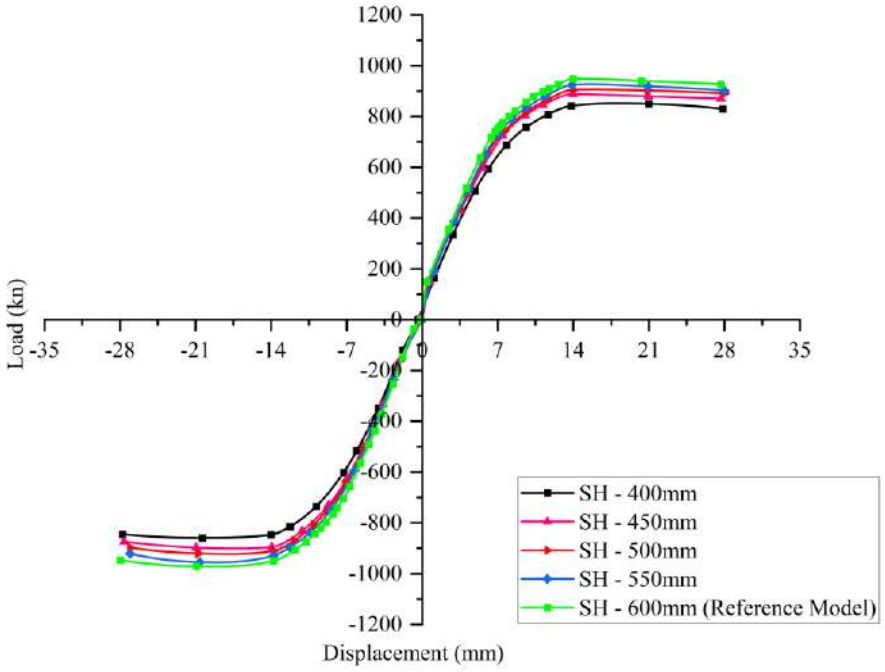

Figure 18: Comparison of hysteretic behavior for different shear spans, with SH-600mm as the reference.

To support design applications, a height-adjusted expression for ultimate load capacity is proposed:

$$P_u = \beta \frac{f_y b {H_e}^2}{4L_e}, \quad \beta \approx 1.08 \tag{5.11}$$

Here, the empirical coefficient β=1.08 accounts for cyclic hardening effects and wall interaction, and is calibrated to match the FE-derived ultimate load for the 600 mm case. This formula enables quick design checks while ensuring compatibility with detailed FE results.

For balanced performance—providing sufficient moment resistance without causing excessive plastic hinge migration—a recommended embedment height range of: $0.8H \leq H_e \leq H$ is proposed, where H is the full depth of the SBsection. This ensures adequate stiffness, energy

dissipation, and ductility, all of which are essential for seismic design.

As shown in Table 8, reducing H_e from 600 mm to 400 mm leads to an approximate 13% decrease in yield load and a 10% decrease in ultimate load under positive loading, with similar reductions observed under reverse loading. This trend arises from the dependence of plastic moment capacity on section geometry, as expressed by:

$$P_y = \frac{M_p}{L_e} = \frac{f_y b {H_e}^2}{L_e} \quad (5.10)$$

When compared to FE-derived results, the analytical estimates using Eq. (5.10) match the simulated yield loads within a 7% margin of error across the studied range, thereby validating the use of the plastic section approach in preliminary design.

The initial secant stiffness $K1 = Py/\Delta y$ also increases with embedment height. A deeper beam section improves the moment of inertia, thereby enhancing the connection's rotational restraint. Between the 600 mm and 400 mm models, a 15% increase in stiffness is observed. This is consistent with prior experimental studies, which have shown that deeper embedment delays the formation of plastic hinges and mitigates early stiffness degradation.

Table 8: Yield and Ultimate Loads of Connections with Different Embedded Heights Under Cyclic Loading.

No	Embedded height /mm	Loading direction	Yield Load (kN)	Relative Ratio	Ultimate Load (kN)	Relative Ratio
SL-0	600	+	874.4	1.00	947.8	1.00
		-	906.2	1.00	971.8	1.00
SH-1	550	+	837.16	0.96	924.4	0.98
		-	896.56	0.99	954.5	0.98
SH-2	500	+	815.6	0.93	904.3	0.95
		-	870.33	0.96	921.1	0.95
SH-3	450	+	804.7	0.92	887.6	0.94
		-	831.01	0.92	897.6	0.92
SH-4	400	+	757.5	0.87	849.41	0.90
		-	814.93	0.90	859.7	0.88

The Von Mises stress contour plot, generated from an Abaqus simulation (likely corresponding to the SH-550 mm model), reveals critical stress concentrations near the connection zones and knee regions. These areas are where stress levels approach or exceed the yield strength [89], indicating the likely initiation of plastic deformation.

Stress distribution patterns—shaped by the connection geometry and deformation mode at the observed load increment—highlight how internal forces are transferred through the connection. While lower stress levels are found farther from the connection interface, the concentration of high stresses around fasteners and steel–concrete interfaces confirms that these zones are pivotal for inelastic deformation and energy dissipation. These findings emphasize the necessity for careful connection detailing to prevent premature failure. Moreover, the associated deformed shape suggests a coupling of bending and distortion effects that shape the observed stress fields. Fully understanding these behaviors requires tracking the connection's stress evolution throughout the entire cyclic loading history—particularly for performance-based seismic design, where controlled yielding is desirable in well-confined regions.

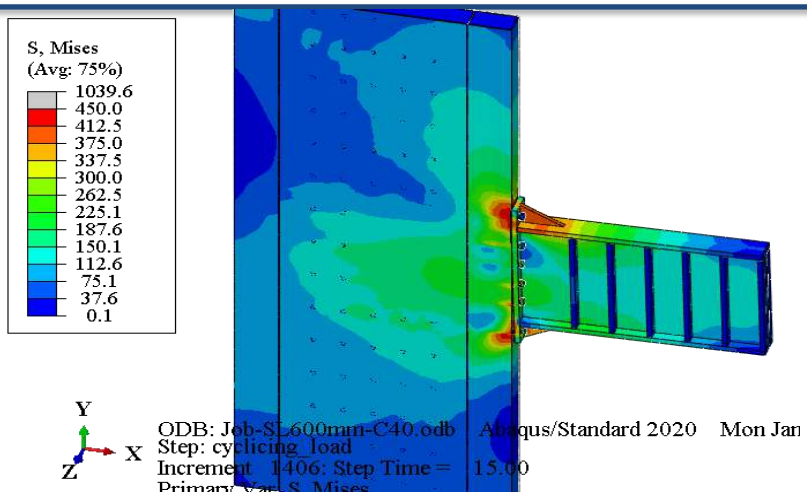

Figure 19: Von Mises stress distribution in a DSCW-SB connection with a Reference embedment height 600mm under cyclic loading, highlighting stress concentrations at the connection interface.

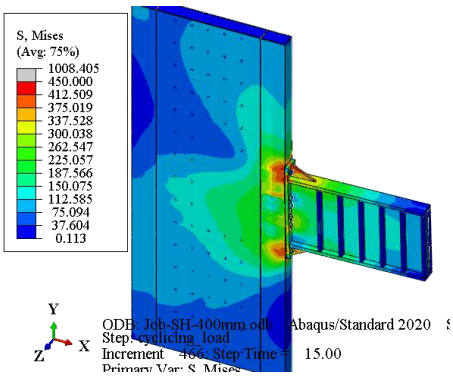

(a) 400mm of height embedded beam

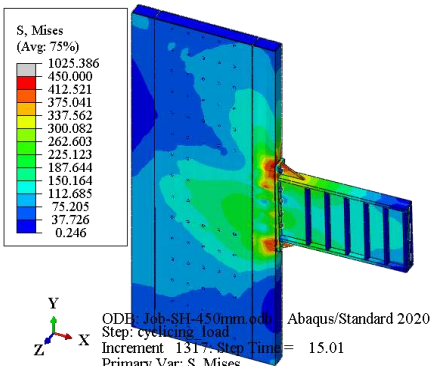

(b) 450mm of height embedded beam

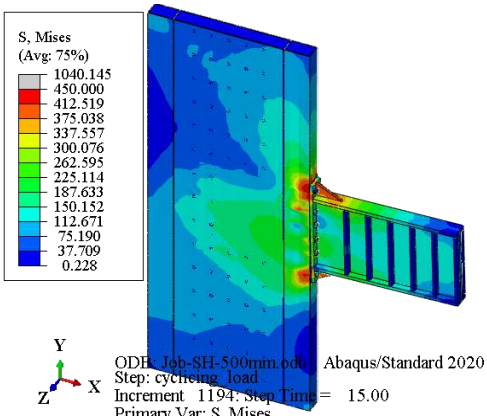

(c) 500mm of height embedded beam

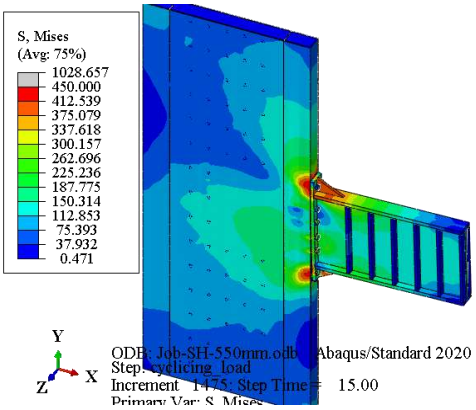

(d) 550mm of height embedded beam

Figure 20: Von Mises stress distribution in a DSCW-SB connection with different embedded beam length under cyclic loading, highlighting stress concentrations at the connection interface.

4.7 Discussion

The results of the parametric finite element (FE) study reveal that embedment geometry plays a decisive role in governing the seismic performance of DSCSW–H-beam connections. In the SL-series, where embedment length was varied from 300 to 700 mm, peak load increased consistently with length, demonstrating a 21.6% improvement between SL-1 (300 mm) and SL-4 (600 mm). However, extending to 700 mm (SL-5) yielded only marginal gains, suggesting diminishing returns. This indicates that excessive embedment length leads to stress concentration and inefficient material use. Hysteresis loops further confirmed that specimens SL-2 and SL-4 exhibited the most stable energy dissipation, with cumulative energy absorption increasing by 27.8% relative to SL-1. These results imply that 500–600 mm represents an optimal embedment range (Hajjar, 2002).

The SH-series, varying embedment height between 250 and 500 mm, highlighted a different trend. Increased embedment height improved initial stiffness, with SH-3 (350 mm) demonstrating 15.4% greater energy dissipation than SH-1 (250 mm). Beyond 400 mm, however, ductility declined significantly, and SH-4 and SH-5 developed brittle shear failure modes. Skeleton curve analysis revealed that higher embedment heights shifted the yield point to larger displacements but reduced post-yield ductility (Gong & Shahrooz, 2001).

Stiffness degradation results corroborated these findings: while longer embedment delayed stiffness loss, excessive height accelerated degradation after the third loading cycle. This dual effect emphasizes that embedment height primarily influences ductility, whereas embedment length governs capacity and energy dissipation (Xu et al., 2022).

The failure patterns observed in FE models also supports these trends. Short embedment lengths caused premature anchorage failure, while overly tall embedment regions forced brittle shear cracking in the concrete core. Optimal models (SL-2, SL-4, SH-2) demonstrated outward plastic hinge development, allowing more favorable energy distribution.

The predictions of the FE to the existing literature of the experimental findings were consistent and the deviation of the capacity was within a range of + 7. This is an attestation of the modeling technique. It is worth noting that the study addresses a gap in knowledge in a very serious manner since it measures the impact of geometry on embedment rather than a qualitative debate.

The findings are presented in simple recommendations, designwise. The ratio of the strength, ductility, and energy dissipation ensures that the embedding length 500-600 mm and the height 300-350 mm are enough to offer seismic resistance of the material under consideration without the material being too expensive. The ranges may serve as some preliminary guidelines of design to the practitioners until the standardized code provisions. Overall, the study is a witness to the fact that the seismic efficiency of DSCSW H-beam connections can be improved with the help of a proper control over the embedment geometry that can be applied both to the research and practice (Zhao et al., 2018).

5 Conclusion and Recommendations.

LThe paper has discussed the effects of embedded beam geometry on seismic behaviour of DSCSW connections between two skin composite shear walls using experimentally validated finite element (FE) models. Two parameters which were varied to check their impact on the strength, ductility, and energy dissipation include embedment length (300-700 mm) and embedment height (250-500 mm) (Li, Wang, and Wu, 2018).

The results confirm that, bearing capacity and energy absorption directly increases with the embedment length but SL-2 (500 mm) and SL-4 (600 mm) exhibit the most stable hysteretic behavior. The final load and the cumulative energy dissipation both rose up to 21.6 and 27.8 percent respectively with length, but beyond length of 600 mm the advantages reduced. Quite the contrary, embedment height had a significant influence on ductility. Even though the 15.4 percentage point difference in dissipation of energy was attained by SH-2 compared to SH-1, the height was excessively high (above 400 mm) causing the concentration of stiffness and brittle shear crackage. These findings were supported by stiffness degradation analysis and skeleton curve analysis that discovered that

balanced embedment dimensions are the only ones that are engaged in optimum performance.

Recommendations

1. Strength and ductility are recommended in design practice as 500-600 mm wide, in terms of embedment length, and 300-350 mm, in terms of height.
2. The designers should not be allowed to make the height of the embedment exceed 400 mm because it reduces the ductility and the loss of stiffness.
3. The additional parametric research on the axial load change and cyclic degradation has a consistent design provided by the experimental FE modeling method.
4. The experimental validation should be expanded in future studies and more information of hybrid embedment should be given so that DSCSW connections can be maximized.

These recommendations provide preliminary guidance for engineers and highlight the potential of DSCSWs as resilient systems in seismic regions.

REFRENCES

Amer, M., Chen, Z. H., Du, Y. S., Mashrah, W. A. H., & Laqsum, S. A. (2025). Axial compression behavior of double-skin composite shear wall with T-stiffener and headed stud connectors. *Advanced Steel Construction*, 21(2), 95–109.

Cai, J., Wang, D., Xu, T., & Huang, L. (2018). Influence of axial compression ratios and shear-span ratios on seismic behavior of composite shear wall with double steel plates and infill concrete with binding bars. *Journal of Building Structure*, 37–43.

Cao, W., Sun, C., & Yang, X. (2008). Experimental study on seismic performance of bidirectional single-row reinforced shear wall joints. *Earthquake Engineering and Engineering Vibration*, (3), 104–109.

Chen, L., Mahmoud, H., Tong, S. M., et al. (2015). Seismic behavior of double steel plate–HSC composite walls. *Engineering Structures*, 102, 1–12.

Cheng, C., Zhang, D., & Zhao, L. (2016). Experimental research on seismic behaviors of low shear-span ratio composite concrete and double steel plate shear walls with binding bars. *Journal of Southeast University*, 126–132.

Dong, H., Li, Y., & Cao, W. (2018). Uniaxial compression performance of rectangular CFST columns with different internal construction characteristics. *Engineering Structures*.

El-Tawil, S., Harries, K. A., Fortney, P. J., et al. (2010). Seismic design of hybrid coupled wall systems: State of the art. *Journal of Structural Engineering*, 136(7), 755–769.

Eom, T. S., Park, H. G., Lee, C. H., et al. (2009). Behavior of double skin composite wall subjected to in-plane cyclic loading. *Journal of Structural Engineering*, 135(10), 1239–1249.

Farsi, A., Keshavarzi, F., Pouladi, P., et al. (2016). Experimental study of a replaceable steel coupling beam with an end-plate connection. *Journal of Constructional Steel Research*, 122, 138–150.

Ge, W., Zhang, Z., Xu, W., Ashour, A., Jiang, H., Sun, C., & Cao, D. (2022). Seismic response of grid tubular-double steel plate concrete composite shear walls and combined system subjected to low reversed cyclic loading. *Engineering Structures*, 256, 114028.

Gong, B., & Shahrooz, B. M. (2001). Concrete–steel composite coupling beams. I: Component testing. *Journal of Structural Engineering*, 127(6), 625–631.

Goswami, R., & Murty, C. V. R. (2010). Externally reinforced welded I-beam-to-box-column seismic connection. *Journal of Engineering Mechanics*, 136(7), 795–804.

Guo, X., Zhang, X., Xu, W., et al. (2022). Seismic tests and simulation of multi-chamber double steel plate composite shear walls. *Concrete and Cement Products*, (3), 71–75.

Hajiaghamohamadi, M., & Mofid, M. (2023). Seismic behavior evaluation of steel infill plate composite shear wall systems

following FEMA P695 methodology. *Asian Journal of Civil Engineering*.

Hajjar, J. F. (2002). Composite steel and concrete structural systems for seismic engineering. *Journal of Constructional Steel Research*, 58(5), 703–723.

Hongwei, L., & Zhifei, S. (2010). Numerical analysis for the out-of-plane response of a reinforced concrete wall beam connection. *International Journal for Computational Methods in Engineering Science and Mechanics*, 11(4), 177–186.

Hossain, K. M. A., & Wright, H. D. (2003). Experimental and theoretical behaviour of composite walling under in-plane shear. *Journal of Constructional Steel Research*, 60(1), 59–83.

Hossain, K. M. A., Rafiei, S., Lachemi, M., et al. (2016). FE modeling of impact shear resistance of double skin composite wall. *Thin-Walled Structures*, 107, 101–118.

Hu, L., Feng, P., Lin, H., Yang, J. Q., & Qiang, H. (2021). Seismic performance of composite shear walls with embedded FCCCs in boundary elements. *Composite Structures*, 257, 113126.

Ji, L., Yong, J., & Xin, L. (2013). Experimental study on the seismic performance of connections of coupling beam and steel reinforced high-strength concrete short-leg shear wall. *Earthquake Engineering and Engineering Vibration*, 33(1), 61–66.

Ji, X., Cheng, Y., Leong, T., et al. (2019). Seismic behavior and strength capacity of steel coupling beam-to-SRC wall connections. *Engineering Structures*, 201, 109820.

Ke, X., Song, Y., Zhang, Z., & Xie, J. (2013). Experimental study on the seismic performance of connections of coupling beam and steel reinforced high-strength concrete short-leg shear wall. *Earthquake Engineering and Engineering Vibration*, (3), 61–66.

Li, G. Q., Gu, F., & Jiang, J. (2017). Cyclic behavior of SB-concrete wall connections with embedded steel columns (I): Experimental study. *Steel and Composite Structures*, 25(3), 257–266.

Li, Z., Wang, W., & Wu, Z. (2018). Analysis on lateral performance of corrugated steel plate composite shear walls. In *Proceedings of the 7th National Conference on Steel Structure Engineering Technology* (pp. 477–481). Zhejiang Zhongnan Construction Group.

Lianguang, J., Yong, J., Xin, L., et al. (2013). Experimental study on the seismic performance of connections of coupling beam and steel reinforced high-strength concrete short-leg shear wall. *Journal of Earthquake Engineering and Engineering Vibration*, 33(1), 61–66.

Link, R. A., & Elwi, A. E. (1995). Composite concrete–steel plate walls: Analysis and behavior. *Journal of Structural Engineering*, 121(2), 260–271.

Liu, A., & Zhou, D. (2005). Experimental study on seismic behavior of semi-rigid connection between steel beam and concrete wall. *Earthquake Engineering and Engineering Vibration*, 25(4), 66–72.

Liu, D., Shi, Y. J., & Yu, X. L. (2013). Experimental study on seismic behavior of modular composite shear wall with double steel plates and infill concrete. *Engineering Mechanics*, 39(8), 111–118.

Lu, X., Yun, C., & Jiang, H. (2018). Earthquake resilience of reinforced concrete structural walls with replaceable components. *Journal of Earthquake Engineering*, 22(5), 801–825.

Ma, X., Jiang, N., & Tong, B. (2013). Numerical model and simplified formula of axial force–moment capacity of composite shear wall with double steel plates and infill concrete. *Journal of Building Structure*, 34(4), 99–106.

Mazlan, Z. H., & Al Zand, A. (2022). Flexural behavior of concrete-filled double-skin hexagonal tubular beams using finite element analysis. *Knowledge-Based Engineering and Sciences*, 3(2), 18–35.

Meng, X., Li, W., & Peng, W. (2015). Seismic performance research of prefabricated wall-

beam connected in-plane. *Journal of Shenyang Jianzhu University (Natural Science)*.

Mirghaderi, S. R., Torabian, S., & Keshavarzi, F. (2010). I-beam to box-column connection by a vertical plate passing through the column. *Engineering Structures*, 32(9), 2804–2812.

Nie, J. G., Ma, X. W., & Tao, M. X. (2014). Effective stiffness of composite shear wall with double plates and filled concrete. *Journal of Constructional Steel Research*, 99, 140–148.

Rafiei, S., Hossain, K. M. A., & Lachemi, M. (2013). FE modeling of double skin profiled composite shear wall system under in-plane loadings. *Engineering Structures*, 56, 46–57.

Shin, K. J., Kim, Y. J., & Oh, Y. S. (2004). Behavior of welded CFT column to steel beam connections with external stiffeners. *Engineering Structures*, 26(13), 1843–1856.

Wan-Shin, P., & Hyun-Do, Y. (2006). Seismic performance of steel coupling beam–wall connections in panel shear failure. *Journal of Constructional Steel Research*, 62(10), 1016–1025.

Wang, S. Y., Chen, A. Y., & Wan, H. Y. (2021). Seismic behaviour of concrete-filled steel tube frames with external composite wall panels. *Advanced Steel Construction*, 17(1), 10–19.

Xu, D., Xiang, B. Q., & Chong, X., et al. (2022). Seismic performances of the connection between replaceable-coupling beams and composite shear wall. *Journal of Constructional Steel Research*, 197, 107462.

Yu, J., Zhao, C., & Zhong, W. (2024). Seismic behavior of partially encased composite columns–steel plate shear wall structure with different semi-rigid connections. *Journal of Building Engineering*, 82(October 2023), 108177.

Zhang, W. Y., Wang, K., & Wang, Q., et al. (2018). Aseismic behavior of composite shear wall with stiffened double steel plates and infilled concrete. *Engineering Mechanics*, 35(11), 125–133.

Zhang, X., & Ricles, J. M. (2006). Seismic behavior of reduced beam section moment connections to deep columns. *Journal of Structural Engineering*, 132(3), 350–358.

Žuvelek, V., Ćurković, I., Lukačević, I., & Rajić, A. (2024, May). Numerical investigation of double-skin cold-formed steel shear wall filled with concrete. In *International Conference "Coordinating Engineering for Sustainability and Resilience"* (pp. 105–115). Cham: Springer Nature Switzerland.